

# Metabolic pathway inference using non-negative matrix factorization with community detection

Abdur Rahman M. A. Basher, Ryan J. McLaughlin, and Steven J. Hallam

May 27, 2020

## Abstract

Machine learning provides a probabilistic framework for metabolic pathway inference from genomic sequence information at different levels of complexity and completion. However, several challenges including pathway features engineering, multiple mapping of enzymatic reactions and emergent or distributed metabolism within populations or communities of cells can limit prediction performance. Here, we present triUMPF, triple non-negative matrix factorization (NMF) with community detection for metabolic pathway inference, that combines three stages of NMF to capture myriad relationships between enzymes and pathways within a graph network followed by community detection to extract higher order structure based on the clustering of vertices sharing similar statistical properties. We evaluated triUMPF performance using experimental datasets manifesting diverse multi-label properties, including Tier 1 genomes from the BioCyc collection of organismal Pathway/Genome Databases and low complexity microbial communities. Resulting performance metrics equaled or exceeded other prediction methods on organismal genomes with improved prediction outcomes on multi-organism data sets.

**Availability and implementation:** The software package, and installation instructions are published on [github.com/triUMPF](https://github.com/triUMPF)

**Contact:** [shallam@mail.ubc.ca](mailto:shallam@mail.ubc.ca)

## 1 Introduction

Pathway reconstruction from genomic sequence information is an essential step in describing the metabolic potential of cells at the individual, population and community levels of biological organization ([3, 17, 12]). Resulting pathway representations provide a foundation for defining regulatory processes, modeling metabolite flux and engineering cells and cellular consortia for defined process outcomes ([23, 11]). The integral nature of the pathway prediction problem has prompted both gene-centric e.g. mapping annotated proteins onto known pathways using a reference database based on sequence homology, and heuristic or rule-based pathway-centric approaches including PathoLogic ([16]) and MinPath ([33]). In parallel, the development of trusted sources of curated metabolic pathway information including the Kyoto Encyclopedia of Genes and Genomes (KEGG) [15] and MetaCyc [7] provides training data for the design of more flexible machine learning (ML) algorithms for pathway inference. While ML approaches have been adopted widely in metabolomics research ([5, 29]) they have gained less traction when applied to predicting pathways directly from annotated gene lists.

Dale and colleagues conducted the first in-depth exploration of ML approaches for pathway prediction using Tier 1 (T1) organismal Pathway/Genome Databases (PGDB) ([6]) from the BioCyc collection randomly divided into training and test sets ([8]). Features were developed based on rule-sets used by the Pathologic algorithm in Pathway Tools to construct PGDBs ([16]). Resulting performance metrics indicated that standard ML approaches rivaled the performance of Pathologic with the added benefit of probability scores ([8]). More recently Basher and colleagues developed multi-label based on logistic regression for pathway prediction (mLGPR), a multi-label classification approach to metabolic pathway inference that uses logistic regression and feature vectors based on the work of Dale and colleagues to predict metabolic pathways from genomic sequence information at different levels of complexity and completion ([3]).

Although mLGPR performed effectively on organismal genomes, pathway prediction outcomes for multi-organismal data sets were less optimal due in part to missing or noisy feature information. In an effort to grapple with this problem, Basher and Hallam evaluated the use of representational learning methods to learn a neural embedding-based low-dimensional space of metabolic features based on a three-layered network architecture consisting of compounds, enzymes, and pathways ([2]). Learned feature vectors improved pathway prediction performance on organismal genomes and motivated the use of graphical models for multi-organismal features engineering.

Here we describe triple non-negative matrix factorization (NMF) with community detection for metabolic pathway inference (triUMPF) combining three stages of NMF to capture relationships between enzymes and pathways within a network ([10]) followed by community detection to extract higher order network structure ([9]). Non-negative matrix factorization is a data reduction and exploration method in which the original

and factorized matrices have the property of non-negative elements with reduced ranks or features ([10]). In contrast to other dimension reduction methods, such as principal component analysis ([4]), NMF both reduces the number of features and preserves information needed to reconstruct the original data ([32]). This has important implications for noise robust feature extraction from sparse matrices including data sets associated with gene expression analysis and pathway prediction ([32]).

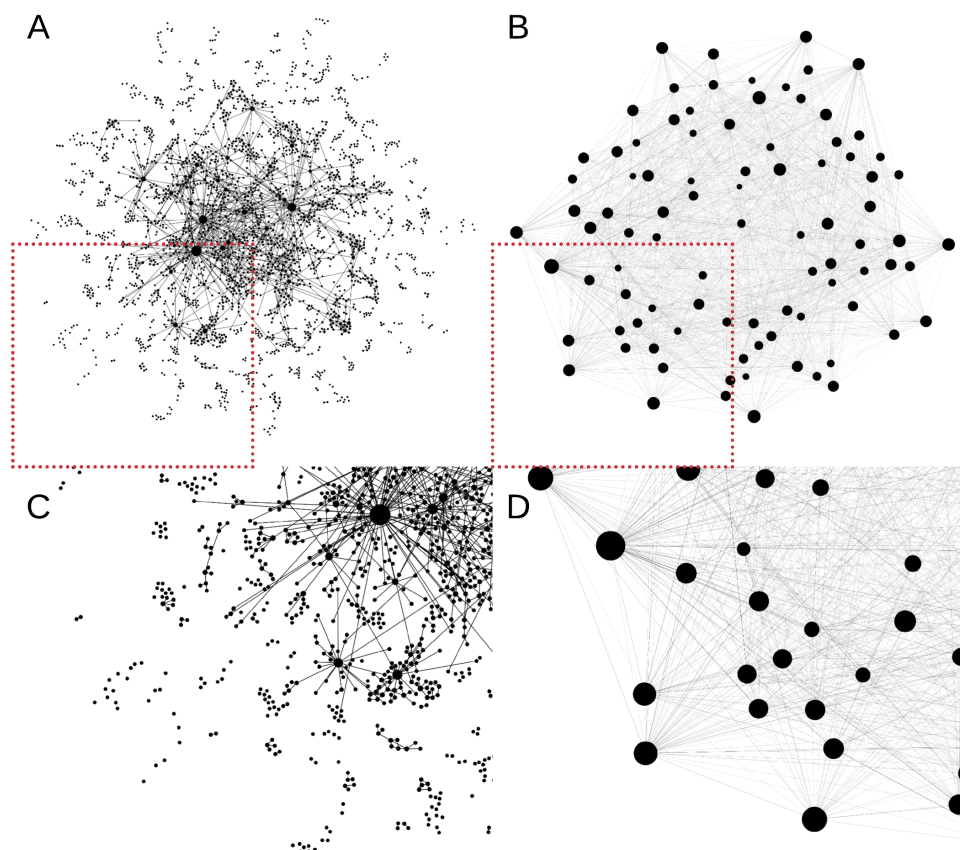


Figure 1: The set of complete metabolic pathways extracted from MetaCyc (A) and their discovered communities (B). Zoomed in region of the pathway-pathway and community-community interactions, C and D respectively. Nodes are metabolic pathways or communities for A,C and B,D respectively. Edges correspond to number of shared enzymatic reactions or shared pathways for the pathway and community nodes respectively.

For pathway prediction, triUMPF uses three graphs, one representing associations between pathways and enzymes indicated by enzyme commission (EC) numbers ([1]), one representing interactions between enzymes and another representing interactions between pathways. The two interaction graphs adopt the *subnetworks* concept introduced in BiomeNet ([27]) and MetaNetSim ([14]), where a subnetwork is a linked series of connected nodes (e.g. reactions and pathways). In the literature, a subnetwork is commonly referred to as a *community* ([25]), which defines a set of densely connected nodes within that subnetwork. Community detection is performed on both interaction graphs to identify subnetworks as shown in Fig. 1A, where a metabolic pathway network, extracted from MetaCyc, is represented as interactions among pathways. The detected pathway communities are illustrated in Fig. 1B. Similar to Fig. 1, enzyme interactions are used to create the enzyme network, which is used to detect enzyme communities.

We evaluated triUMPF parameter sensitivity, robustness and prediction performance in relation to other inference methods including Pathologic, MinPath and mlGPR on a set of T1 PGDBs and low complexity microbial communities including symbiont genomes encoding distributed metabolic pathways for amino acid biosynthesis [20], genomes used in the Critical Assessment of Metagenome Interpretation (CAMI) initiative [26], and whole genome shotgun sequences from the Hawaii Ocean Time Series (HOTS) [28].

## 2 Definitions and Problem Formulation

Here, the default vector is considered to be a column vector and is represented by a boldface lowercase letter (e.g.,  $\mathbf{x}$ ) while matrices are represented by boldface uppercase letters (e.g.,  $\mathbf{X}$ ). The  $\mathbf{X}_i$  matrix indicates the  $i$ -th row of  $\mathbf{X}$  and  $\mathbf{X}_{i,j}$  denotes the  $(i, j)$ -th entry of  $\mathbf{X}$  while, for a vector,  $\mathbf{x}_i$  denotes an  $i$ -th cell of  $\mathbf{x}$ . The transpose of  $\mathbf{X}$  is denoted as  $\mathbf{X}^\top$  and the trace of it is symbolized as  $\text{tr}(\mathbf{X})$ . The Frobenius norm of  $\mathbf{X}$  is defined as  $\|\mathbf{X}\|_F = \sqrt{\sum_{i \in n} \sum_{j \in m} \mathbf{X}_{i,j}^2}$ . Occasional superscript,  $\mathbf{X}^{(i)}$  (or  $\mathbf{x}^{(i)}$ ), suggests an index to a sample, a power, or a current epoch during a learning period. We use calligraphic letters to represent sets (e.g.,  $\mathcal{E}$ ) while we use the notation  $|\cdot|$  to denote the cardinality of a given set. With these notations in mind, we introduce several concepts integral to the problem formulation.

Metabolic pathway inference from genomic sequence information at different levels of complexity and completion requires a trusted source of labeled pathway information in which the set of ordered reactions within and between cells is linked to substrates and products (compounds or metabolites). This information can be represented in graphs corresponding to reactome and pathway-level interactions. In this study, we use MetaCyc, a multi-organism member of the BioCyc collection of Pathway/Genome Databases (PGDB) as the trusted source for reactome and pathway information [6]. MetaCyc contains only experimentally validated metabolic pathways across all domains of life. To simplify computational complexity, we consider the reaction and pathway graphs to be undirected.

**Definition 2.1. Reaction Graph Topology.** Let the reaction graph be represented by an undirected graph  $\mathcal{G}^{(\text{rxn})} = \{\mathcal{C}, \mathcal{Z}^{(c)}\}$ , where  $\mathcal{C}$  is a set of  $c$  metabolites and  $\mathcal{Z}^{(c)}$  represents  $r'$  links between compounds. Each link indicates a reaction, derived from a set of biochemical reactions  $\mathcal{R}$  of size  $r'$ . Then, the reaction graph topology is defined by a matrix  $\Omega^{(c)} \in \mathbb{Z}_{\geq 0}^{r' \times c}$ , where each entry  $\Omega_{i,j}^{(c)}$  is a binary value of 1 or 0, indicating either the compound  $j$  is a substrate/product in a reaction  $i$  or not involved in that reaction, respectively. ■

**Definition 2.2. Pathway Graph Topology.** Let  $\mathcal{G}^{(\text{path})} = \{\mathcal{R}, \mathcal{Z}^{(r)}\}$  be an undirected graph, where  $\mathcal{R}$  is presented in Definition 2.1, and  $\mathcal{Z}^{(r)}$  represents a set of  $t'$  links between reactions. Then, the pathway graph topology is defined by a matrix  $\Omega^{(r)} \in \mathbb{Z}_{\geq 0}^{t' \times r'}$ , where each entry  $\Omega_{i,j}^{(r)}$  is either 0 or a positive integer, corresponding to the absence or the frequency of the reaction  $j$  in pathway  $i$ , respectively. And,  $t$  is the number of pathways in a set  $\mathcal{T}$ . ■

Note that reactions in  $\mathcal{G}^{(\text{path})}$  may be annotated as a *spontaneous reaction* or a reaction catalyzed by one or more enzymes, *enzymatic reaction* and classified by an *enzyme commission number* (EC) ([21]). In addition, a number of enzymes referred to as *promiscuous enzymes* can participate in more than one pathway. Given this information we associate EC numbers to pathways and formulate three graphs, one representing associations between pathways and enzymes indicated by enzyme commission (EC) numbers  $\mathbf{M} \in \mathbb{Z}_{\geq 0}^{t \times r}$ , one representing interactions between enzymes  $\mathbf{B} \in \mathbb{Z}_{\geq 0}^{r \times r}$  and another representing interactions between pathways  $\mathbf{A} \in \mathbb{Z}_{\geq 0}^{t \times t}$  (see Supp. Section 1). After determining relationships within each graph, we define a *multi-label* metabolic pathway dataset.

**Definition 2.3. Multi-label Pathway Dataset** ([3]). A general form of pathway dataset is characterized by  $\mathcal{S} = \{(\mathbf{x}^{(i)}, \mathbf{y}^{(i)}) : 1 < i \leq n\}$  consisting of  $n$  examples, where  $\mathbf{x}^{(i)}$  is a vector indicating the abundance information corresponding to each enzymatic reaction. An enzymatic reaction, in turn, is denoted by  $e$ , which is an element of a set of enzymatic reactions  $\mathcal{E} = \{e_1, e_2, \dots, e_r\}$ , having  $r$  possible reactions. The abundance of an enzymatic reaction  $i$ , for example  $e_i^{(i)}$ , is defined as  $a_i^{(i)} (\in \mathbb{R}_{\geq 0})$ . The class labels  $\mathbf{y}^{(i)} = [y_1^{(i)}, \dots, y_t^{(i)}] \subseteq \{-1, +1\}^t$  is a pathway label vector of size  $t$  that represents the total number of pathways, which are derived from a set of labeled metabolic pathway  $\mathcal{Y}$ . The matrix form of  $\mathbf{x}^{(i)}$  and  $\mathbf{y}^{(i)}$  are symbolized as  $\mathbf{X}$  and  $\mathbf{Y}$ , respectively. ■

The input space is assumed to be encoded as  $r$ -dimensional feature vector and is symbolized as  $\mathcal{X} = \mathbb{R}^r$ . Furthermore, each example in  $\mathcal{S}$  is considered to be drawn independent, identically distributed (i.i.d) from an unknown distribution  $\mathcal{D}$  over  $\mathcal{X} \times 2^{|\mathcal{Y}|}$ .

**Problem Statement 1. Metabolic Pathway Prediction.** Given: i)- Pathway-EC matrix  $\mathbf{M}$ , ii)- a Pathway-Pathway interaction matrix  $\mathbf{A}$ , iii)- an EC-EC interaction matrix  $\mathbf{B}$ , and iv)- a dataset  $\mathcal{S}$ , the goal is to efficiently reconstruct pathway labels for a hitherto unseen instance  $\mathbf{x}^*$ .

## 3 The triUMPF Method

In this section, we provide a description of triUMPF components, presented in Fig 2, including: i)- decomposing the pathway EC association matrix, ii)- subnetwork or community reconstruction, and iii)- the multi-label learning process.

### 3.1 Decomposing the Pathway EC Association Matrix

Inspired by the idea of non-negative matrix factorization (NMF), we decompose the P2E association matrix to recover low-dimensional latent factor matrices ([10]). Unlike previous application of NMF to biological data sets ([22]), triUMPF incorporates learned embeddings into the matrix decomposition process. Formally, given

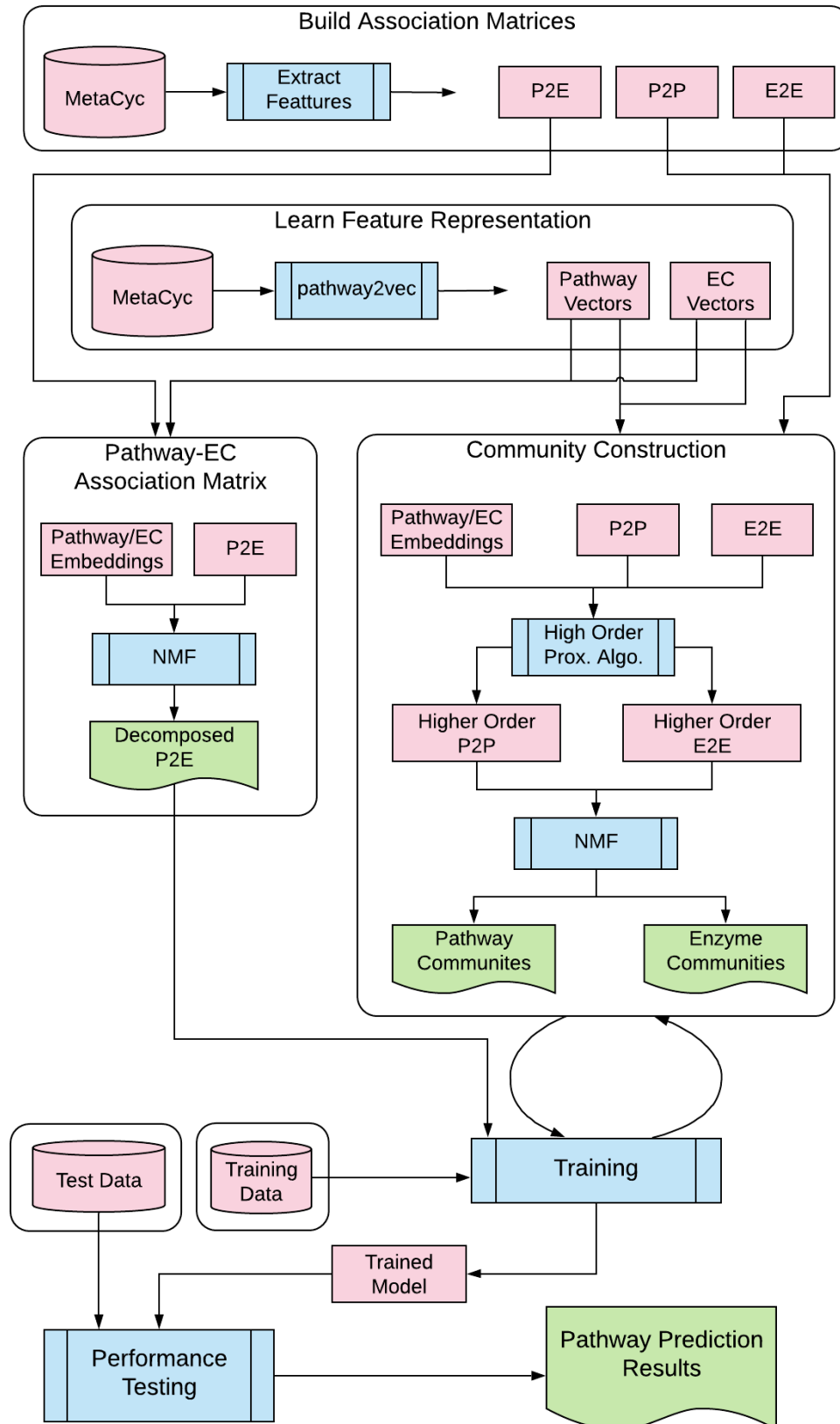


Figure 2: A workflow diagram showing the proposed triUMPF method, where the model takes two graph topology, corresponding Pathway-Pathway interaction and EC-EC interaction, and a dataset to detect pathway and EC communities while, simultaneously, decomposing Pathway-EC association information to produce a constrained low rank matrix. Afterwards, a set of pathways is detected from a newly annotated genome or metagenome.

the non-negative  $\mathbf{M}$  standard NMF decomposes the matrix into the two low-rank matrices, i.e.  $\mathbf{M} \approx \mathbf{W}\mathbf{H}^\top$ , where  $\mathbf{W} \in \mathbb{R}^{t \times k}$  stores the latent factors for pathways while  $\mathbf{H} \in \mathbb{R}^{r \times k}$ , known as the basis matrix, can be thought of as latent factors associated with ECs and  $k \ll t, r$ . We extend standard NMF by incorporating the two constraints: i)- interactions within ECs or pathways and ii)- interactions between pathways and ECs. For this, we apply the *pathway2vec* framework ([2]) to extract features in the form of continuous vectors, for each EC and pathway while incorporating interaction constraints. This set of features can then be used to obtain the following minimization objective function:

$$\begin{aligned} \mathcal{J}^{\text{fact}}(\mathbf{W}, \mathbf{H}, \mathbf{U}, \mathbf{V}) = & \min_{\mathbf{W}, \mathbf{H}, \mathbf{U}, \mathbf{V}} \|\mathbf{M} - \mathbf{W}\mathbf{H}^\top\|_F^2 + \lambda_1 \|\mathbf{W} - \mathbf{P}\mathbf{U}\|_F^2 \\ & + \lambda_2 \|\mathbf{H} - \mathbf{E}\mathbf{V}\|_F^2 + \lambda_3 \|\mathbf{U} - \mathbf{V}\|_F^2 \\ & + \lambda_4 (\|\mathbf{W}\|_F^2 + \|\mathbf{H}\|_F^2 + \|\mathbf{U}\|_F^2 + \|\mathbf{V}\|_F^2) \\ \text{s.t. } & \{\mathbf{W}, \mathbf{H}, \mathbf{U}, \mathbf{V}\} \geq 0 \end{aligned} \quad (3.1)$$

where  $\lambda_*$  are regularization hyperparameters. The leftmost term is the well-known squared loss function that penalizes the deviation of the estimated entries in both  $\mathbf{W}$  and  $\mathbf{H}$  from the true association matrix  $\mathbf{M}$ . The second term corresponds to the relative differences of latent matrix  $\mathbf{W}$  from the pathway features  $\mathbf{P} \in \mathbb{R}^{t \times m}$ , learned using *pathway2vec* framework, where the matrix  $\mathbf{U} \in \mathbb{R}^{m \times k}$  absorbs different scales of matrices  $\mathbf{W}$  and  $\mathbf{P}$ . Similarly, the third term indicates the squared loss of  $\mathbf{H}$  from  $\mathbf{E} \in \mathbb{R}^{r \times m}$ , which denotes the feature matrix of ECs, and their differences are captured by  $\mathbf{V} \in \mathbb{R}^{m \times k}$ . In the fourth term, we minimize the differences between factors  $\mathbf{U}$  and  $\mathbf{V}$ , capturing the shared prominent features for the low dimensional coefficients.

### 3.2 Subnetwork or Community Reconstruction

Graph abstraction is a process of reducing a set of linked nodes into a more compact form, such as isolating densely connected nodes that possess similar properties or functions. The task of discovering distinct group of nodes is known as the community detection problem ([25, 19]). Motivated by this work, we use community detection to guide the learning process for pathways on the two adjacency matrices  $\mathbf{A}$  and  $\mathbf{B}$ , indicating P2P and E2E associations, respectively. For example, Fig. 1 shows 90 communities in pathway network, where the intra-group of nodes, within a community, interacts with each other more frequently than with those outside the group.

The two matrices  $\mathbf{A}$  and  $\mathbf{B}$  represent first-order proximity, capturing pairwise proximity among their related vertices ([30]). However, as discussed in ([25]), the first-order proximity is inadequate to fully characterize distant relationships among pathways or ECs. As such, higher-order, in particular second and third order, proximity is pursued, which can be obtained using the formula ([19]):

$$\mathbf{A}^{\text{prox}} = \sum_{i \in l_p} \omega_i \mathbf{A}^i, \quad \mathbf{B}^{\text{prox}} = \sum_{i \in l_e} \gamma_i \mathbf{B}^i \quad (3.2)$$

where  $\mathbf{A}^{\text{prox}}$  and  $\mathbf{B}^{\text{prox}}$  are polynomials of order  $l_p$  and  $l_e$ , respectively, and  $\omega$  and  $\gamma$  are weights associated to each term. Using these higher order matrices, we invoke NMF to recover communities.

Formally, let  $\mathbf{T} \in \mathbb{R}^{m \times p}$  be a non-negative community representation matrix of size  $p$  communities for pathways, where the  $j$ -th column in  $\mathbf{T}_{:,j}$  denotes the representation of community  $j$ . The pathway community indicator matrix is denoted by  $\mathbf{C} \in \mathbb{R}^{t \times p}$  conditioned on  $\text{tr}(\mathbf{C}^\top \mathbf{C}) = t$ , where each entry  $\mathbf{C}_{i,l}$  and  $\mathbf{C}_{j,l}$  encodes the probability that pathways  $i$  and  $j$  generates an edge belonging to a community  $l$ . The probability of  $i$  and  $j$  belonging to the same community can be assessed as:  $\overline{\mathbf{A}}_{i,j}^{\text{prox}} = (\mathbf{P}_i \mathbf{C}_{:,l} \mathbf{T}_{l,i}^\top)^\top (\mathbf{P}_j \mathbf{C}_{:,l} \mathbf{T}_{l,j}^\top)$ . Similar discussion follows for the non-negative representation matrix  $\mathbf{R} \in \mathbb{R}^{m \times v}$  and the EC community indicator matrix  $\mathbf{K} \in \mathbb{R}^{r \times v}$  of  $v$  communities, conditioned on  $\text{tr}(\mathbf{K}^\top \mathbf{K}) = r$ . Unfortunately, due to the constraints emphasized on  $\mathbf{C}$  and  $\mathbf{K}$ , it is not straightforward to analytically derive an expression, instead, we resort to much more tractable solution provided in ([30]), and relax the condition to be an orthogonal constraint, resulting in the following objective function:

$$\begin{aligned} \mathcal{J}^{\text{comm}}(\mathbf{C}, \mathbf{K}) = & \min_{\mathbf{C}, \mathbf{K}} \|\mathbf{A}^{\text{prox}} - \mathbf{P}\mathbf{T}\mathbf{C}^\top\|_F^2 \\ & + \|\mathbf{B}^{\text{prox}} - \mathbf{E}\mathbf{R}\mathbf{K}^\top\|_F^2 \\ & + \alpha \|\mathbf{C}^\top \mathbf{C} - \mathbf{I}\|_F^2 + \beta \|\mathbf{K}^\top \mathbf{K} - \mathbf{I}\|_F^2 \\ & + \lambda_5 (\|\mathbf{C}\|_F^2 + \|\mathbf{K}\|_F^2) \\ \text{s.t. } & \{\mathbf{C}, \mathbf{K}\} \geq 0 \end{aligned} \quad (3.3)$$

where  $\mathbf{I}$  denotes an identity matrix,  $\lambda_5$  is a regularization hyperparameter while  $\alpha$  and  $\beta$  are both positive hyperparameters. The value of these hyperparameters is usually set to a large number, e.g.  $10^9$  in this work, for adjusting the contribution of corresponding terms. The obtained communities in Eq 3.3 are directly linked to the underlying graph topologies, i.e.,  $\mathbf{A}^{\text{prox}}$  and  $\mathbf{B}^{\text{prox}}$ . Because our primary goal is to explore communities from data, based on these graph structures we extend the formula by merging data into the community detection process in the next section.

	#EC	#Compound	#Pathway	$ \mathcal{V} $	$ \mathcal{E} $
MetaCyc (uec)	6378	13689	2526	22593	33353
<b>M</b>	3650	–	2526	–	8576
<b>A</b>	–	–	2526	–	9938
<b>B</b>	3650	–	–	–	35629

Table 1: Characteristics of MetaCyc database and the three association matrices. MetaCyc (uec) denotes enzymatic reactions where links among enzymatic reactions are removed. The “–” indicates non applicable operation.

### 3.3 Multi-label Learning Process

We now bring together the NMF and community detection steps with multi-label classification for pathway prediction. The learning problem must obey rules mandated by **M** while being lenient towards the dataset  $\mathcal{S}$ , which should provide enough evidence to generate representations of communities among pathways and ECs, as suggested by  $\mathbf{A}^{\text{prox}}$  and  $\mathbf{B}^{\text{prox}}$ . We present a weight term  $\Theta \in \mathbb{R}^{t \times r}$  that enforces  $\mathbf{X}$  to be close enough to both **Y** and **M**. We also introduce two auxiliary terms  $\mathbf{L} \in \mathbb{R}^{n \times m}$ , which capture correlations between  $\mathbf{X}$  and **Y** and  $\mathbf{Z} \in \mathbb{R}^{r \times r}$ , enforcing the pathway coefficients associated with **M** resulting in the following objective function:

$$\begin{aligned}
 \mathcal{J}^{\text{path}}(\mathbf{T}, \mathbf{R}, \Theta, \mathbf{L}, \mathbf{Z}) = & \min_{\mathbf{T}, \mathbf{R}, \Theta, \mathbf{L}, \mathbf{Z}} \sum_{i \in n} \sum_{k \in t} \log \left( 1 + e^{-y_k^{(i)} \Theta_k^T \mathbf{x}^{(i)}} \right) \\
 & + \|\mathbf{X} - \mathbf{LRK}^T\|_F^2 + \|\mathbf{Y} - \mathbf{LTC}^T\|_F^2 \\
 & + \rho \|\Theta - \mathbf{ZHW}^T\|_F^2 \\
 & + \lambda_5 (\|\mathbf{T}\|_F^2 + \|\mathbf{R}\|_F^2) \\
 & + \lambda_6 (\|\Theta\|_{2,1} + \|\mathbf{L}\|_F^2 + \|\mathbf{Z}\|_F^2) \\
 \text{s.t. } & \{\mathbf{T}, \mathbf{R}\} \geq 0
 \end{aligned} \tag{3.4}$$

where  $\lambda_5$ ,  $\lambda_6$ , and  $\rho$  are regularization hyperparameters, and  $\|\cdot\|_{2,1}$  represents the sum of the Euclidean norms of columns of a matrix introduced to emphasize sparseness. Notice that we do not restrict the terms **L** and **Z** to be non-negative. Both the second and the third terms in Eq. 3.4, are needed to discover pathway and EC communities, i.e., **C** and **K**, respectively.

The Eqs 3.1, 3.3, and 3.4 are jointly non-convex due to non-negative constraints on the original and the approximation factorized matrices, implying the solutions to triUMPF are only unique up to scalings and rotations ([32]). Hence, we adopt an alternating optimization algorithm to solve each objective function simultaneously, which is provided in Supp. Section 2.

## 4 Experimental Setup

Here, we describe the experimental framework used to demonstrate triUMPF pathway prediction performance across multiple datasets spanning the genomic information hierarchy ([3]). triUMPF was implemented in the Python programming language (v3). Unless otherwise specified all tests were conducted on a Linux server using 10 cores of Intel Xeon CPU E5-2650.

### 4.1 Association Matrices

MetaCyc was used to obtain the three association matrices, P2E (**M**), P2P, (**A**), and E2E (**B**). Some of the properties for each matrix are summarized in Table 1. All three matrices are extremely sparse. For example, **M** contains 2526 pathways, having an average of four EC associations per pathway, leaving more than 3600 columns with zero values.

### 4.2 Pathway and Enzymatic Reaction Features

The pathway and EC features, indicated by **P** and **E**, respectively, were obtained using pathway2vec ([2]). The following settings were applied to learn pathway and EC features: the embedding method was “cm2v” while the meta-path scheme was “ECTCE”, the number of sampled path instances was 100, the walk length is 100, the embedding dimension size was  $m = 128$ , the neighborhood size was 5, the size of negative samples was 5, and the used configuration of MetaCyc was “uec”, indicating links among ECs are being trimmed. The pattern “ECTCE” describes two-level interactions between enzymatic reactions (E) with compounds (C) and compounds with pathways (T).

### 4.3 Description of Datasets

We evaluated triUMPF performance using a corpora of 10 experimental datasets manifesting diverse multi-label properties, including manually curated organismal genomes and low complexity microbial communities including symbiont genomes encoding distributed metabolic pathways for amino acid biosynthesis ([20]), Critical Assessment of Metagenome Interpretation (CAMI) initiative low complexity dataset consisting of 40 genomes ([26]) and whole genome shotgun sequences from the Hawaii Ocean Time Series (HOTS) at 25m, 75m, 110m (sunlit) and 500m (dark) ocean depth intervals ([28]). General statistics about the datasets are summarized in Supp. Table 1. For training we used BioCyc (v20.5 tier 2 & 3) ([6]) consisting of 9255 PGDBs (Pathway/Genome Databases) constructed using Pathway Tools v21 ([16]). Less than 1460 trainable pathways were recoverable from this version of BioCyc. To offset this limit, we concatenated EC features to the original input EC space to leverage correlations among ECs during training (see Supp. Section 4).

### 4.4 Parameter Settings

For training, unless otherwise indicated, the learning rate was set to 0.0001, batch size to 50, number of epochs to 10, number of components  $k = 100$ , number of pathway and EC communities to  $p = 90$  and  $v = 100$ , respectively. The higher-order proximity for  $\mathbf{A}^{\text{prox}}$  and  $\mathbf{B}^{\text{prox}}$  were set  $l^p = 3$  and  $l^e = 1$  and their associated weights fixed as  $\omega = 0.1$  and  $\gamma = 0.3$ , respectively. The  $\alpha$  and  $\beta$  were fixed to  $10^9$ . For the regularized hyperparameters  $\lambda_*$ , we performed 10-fold cross-validation on a subsampled of BioCyc data and found the settings  $\lambda_{1.5} = 0.01$ ,  $\lambda_6 = 10$ , and  $\rho = 0.001$  to be optimum on T1 golden datasets. Hence, we recommend these configurations for triUMPF trained using MetaCyc.

## 5 Experimental Results and Discussion

Four consecutive tests were performed to ascertain the performance of triUMPF including parameter sensitivity, network reconstruction, visualization, and metabolic pathway prediction effectiveness.

### 5.1 Parameter Sensitivity

**Experimental setup.** The impact of seven hyperparameters ( $k, p, v, l_p, l_e, \omega$  and  $\gamma$ ) was evaluated in relation to reconstruction cost of the associated matrices ( $\mathbf{M}$ ,  $\mathbf{A}^{\text{prox}}$ , and  $\mathbf{B}^{\text{prox}}$ ). The reconstruction cost (or error) defines the sum of mean squared errors accounted in the process of transforming the decomposed matrices into its original form where lower cost entails the decomposed low dimensional matrices were able to better capture the representations of the original matrix. We specifically evaluated the effects of varying the following parameters: i)- the number of components  $k \in \{20, 50, 70, 90, 120\}$ , ii)- the community size of pathway  $p \in \{20, 50, 70, 90, 100\}$  and EC  $v \in \{20, 50, 70, 90, 100\}$ , iii)- the higher-order proximity  $l_p$  and  $l_e \in \{1, 2, 3\}$ , and iv)- weights of the polynomial order  $\omega$  and  $\gamma \in \{0.1, 0.2, 0.3\}$ . We used the full matrix  $\mathbf{M}$ , for each test, however, for community detection, we used BioCyc data that is divided into training (80%), validation (5%) and test sets (15%). The final costs for community detection are reported based on the test set after 10 successive trials. In addition, we contrast triUMPF with the standard NMF for monitoring the reconstruction costs of  $\mathbf{M}$  by varying  $k$  values.

**Experimental results.** Supp. Fig. 1 shows the effect of rank  $k$  on triUMPF performance. In general, we observe that the performance is steady with the increase of  $k$ . This is in contrast to standard NMF where the reconstruction cost decreases as the number of features increases. This is expected because, unlike standard NMF, triUMPF exploits two types of correlations to recover  $\mathbf{M}$ : i)- within ECs or pathways and ii)- betweenness interactions, hence, serving as additional regularizers. As observed from Supp. Fig. 1, higher  $k$  values result in improved outcomes. Consequently, we selected  $k = 100$  for performing downstream testing.

For community detection, we observed optimal results with respect to pathway community size at  $p = 20$  under parameter settings  $k = 100$  and  $v = 100$ , as shown in Supp. Fig. 2a. However, because  $\mathbf{A}^{\text{prox}}$  is so sparse, we suggest that this low rank may not correspond to the optimum community size. As with all methods of community detection triUMPF is sensitive to community size and requires empirical testing. There, we tested settings between  $p = 20$  and  $p = 100$  and observed a decrease in performance under parameter settings  $k = 100$  and  $v = 100$  with  $p = 90$  providing a balance between cost and increased community size. A similar result was observed for EC community size at  $v = 100$  under parameter settings  $p = 90$  and  $k = 100$  in Fig. Supp. Fig. 2a.

Finally, we show the effect of changing polynomial orders, and their weights on triUMPF performance. From Supp. Fig. 2c, we see that the reconstruction error progressively increases with varying higher orders for all the three weights  $\omega$ . However, for the same reasons described above, we prefer more long distances with less weight to preserve community structure, and remarkably, when  $\omega = 0.1$  triUMPF performance was relatively stable after the second order. The same conclusion can be drawn for  $l_e$  and its associated weights  $\gamma$  in Supp. Fig. 2d.

Based on these results, triUMPF performance (under MetaCyc v21) is stable while minimizing cost under the following parameter settings:  $k = 100$ ,  $p > 90$ ,  $e > 90$ ,  $l_p = 3$ ,  $\omega = 0.1$ ,  $l_e = 1$ , and  $\gamma = 0.3$ .

## 5.2 Network Reconstruction

**Experimental setup.** We next examined the robustness of triUMPF when exposed to noise. Links were randomly removed from  $\mathbf{M}$ ,  $\mathbf{A}$ , and  $\mathbf{B}$  according to  $\varepsilon \in \{20\%, 40\%, 60\%, 80\%\}$ . We used the partially linked matrices to refine parameters while comparing the reconstruction cost against the full association matrices  $\mathbf{M}$ ,  $\mathbf{A}$  and  $\mathbf{B}$ . Specifically for  $\mathbf{M}$ , we varied components of  $\mathbf{M}$  according to  $k \in \{20, 50, 70, 90, 120\}$  along with  $\varepsilon$ . For all experiments, BioCyc was used for training using the hyperparameters described in Section 4.4.

**Experimental results.** Supp. Fig. 3a indicate that by progressively increasing noise  $\varepsilon$  to  $\mathbf{M}$ , the reconstruction cost increases when  $k$  is low. As more features are incorporated the cost at all noise levels steadily decreases up to  $k = 100$ . This tendency indicates that both pathway and EC features ( $\mathbf{P}$  and  $\mathbf{E}$ ) contain useful correlations that contribute to the resilience of triUMPF's performance when  $\mathbf{M}$  is perturbed.

For  $\mathbf{A}^{\text{prox}}$  and  $\mathbf{B}^{\text{prox}}$ , as shown in Supp Figs 3b and 3c, the costs are reduced in the presence of noise, which is not surprising as the reconstruction of associated communities are constrained on both data and  $\mathbf{A}^{\text{prox}}$  and  $\mathbf{B}^{\text{prox}}$ . These results are directly linked to the sparseness of both matrices, as previously described in ([9]). The pathway graph network, depicted in Fig. 1, indicates that many pathways constitute islands with no direct links, while some pathways are densely connected. For community detection, it is sufficient to group nodes that are densely connected, while links between communities can remain sparse. The same line of reasoning follows for the EC network.

## 5.3 Visualization

**Experimental setup.** Recall that community detection was used to guide the learning process using BioCyc T2 &3. Under circumstances where BioCyc T2 &3 are excluded from Eq. 3.4, triUMPF identifies pathway communities from  $\mathbf{A}$  defined according to MetaCyc. However, when trained with BioCyc T2 &3 connected pathways may be distributed across multiple communities. This happens due to the heterogeneous nature of the BioCyc collection and presents an opportunity to evaluate the statistical properties of pathway communities in relation to both taxonomic and functional diversity within the training set.

To explore these properties in more detail, we visualized MetaCyc and BioCyc communities associated with the tricarboxylic acid (TCA) cycle. The TCA cycle represents a series of reactions central to cellular metabolism and can be found in different forms called pathway variants in aerobic and anaerobic organismal genomes. We then visualized the impact of community detection on pathway prediction by comparing metabolic networks predicted for *E. coli* K-12 substr. MG1655 (TAX-511145), uropathogenic *E. coli* str. CFT073 (TAX-199310), and enterohemorrhagic *E. coli* O157:H7 str. EDL933 (TAX-155864) using both PathoLogic (taxonomic pruning) and triUMPF. All experiments were conducted based on the settings in Section 4.4.

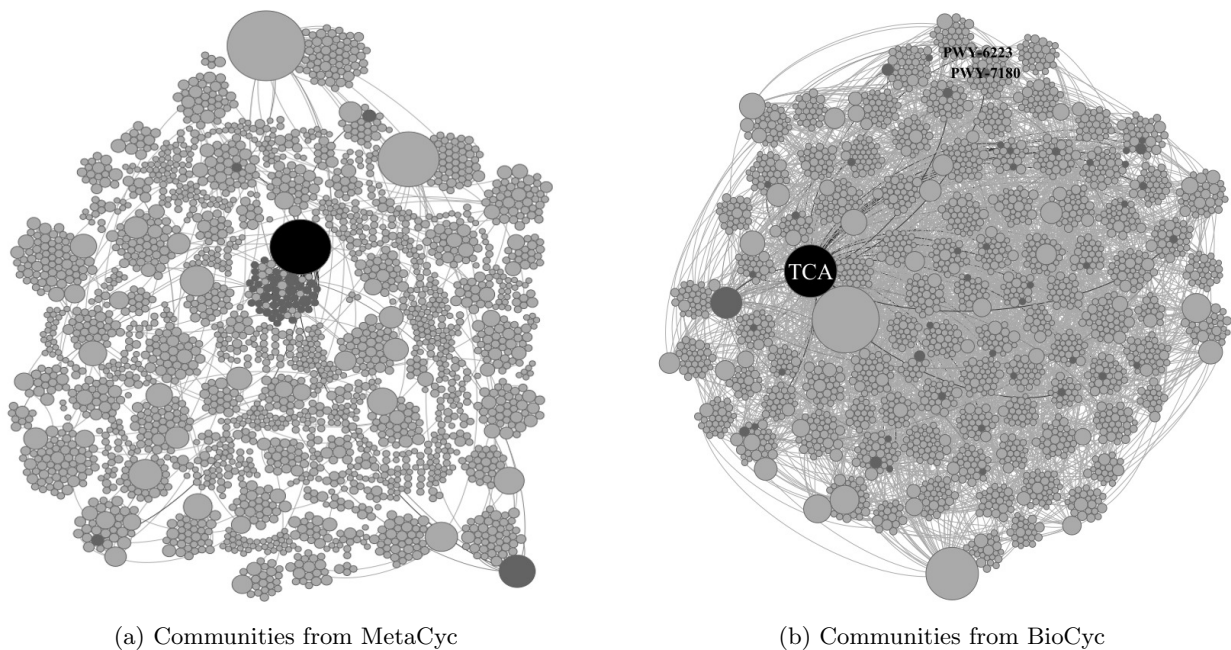


Figure 3: TCA cycle and associated pathways. Pathway communities visualized with and without training using BioCyc T2 &3. (a) MetaCyc communities and (b) BioCyc communities detected using triUMPF. Nodes coloured black indicate the *TCA cycle* (TCA) while dark grey nodes indicate associated pathways. Remaining pathway communities not associated with the TCA cycle are indicated in light grey. PWY-7180: 2-deoxy- $\alpha$ -D-ribose 1-phosphate degradation; PWY-6223: gentisate degradation I.



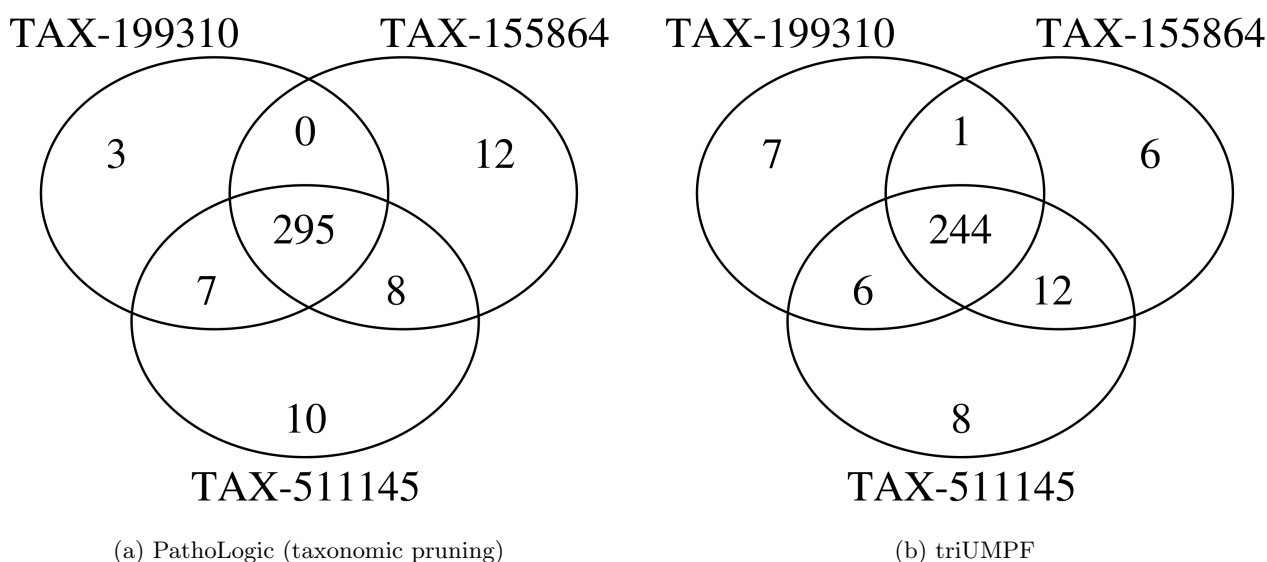


Figure 4: A three way set difference analysis of pathways predicted for *E. coli* K-12 substr. MG1655 (TAX-511145), *E. coli* str. CFT073 (TAX-199310), and *E. coli* O157:H7 str. EDL933 (TAX-155864) using (a) PathoLogic (taxonomic pruning) and (b) triUMPF.

**Experimental results.** Fig. 3a shows pathway communities obtained using MetaCyc, where pathways associated with the *TCA cycle* grouped together in the graph according to  $\mathbf{A}^{\text{prox}}$ . For example, the *pyruvate decarboxylation to acetyl CoA* pathway that converts pyruvate to acetyl-CoA as input to the *TCA cycle* was identified in the same *TCA* community. In contrast, triUMPF trained using BioCyc T2 & 3 assigned *TCA* associated pathways to several distinct communities as exhibited in Fig. 3b. For example, the pathways *2-deoxy- $\alpha$ -D-ribose 1-phosphate degradation* that produces inputs to glycolysis (D-glyceraldehyde-3-phosphate) and *TCA cycle* (acetyl-coA), and *gentisate degradation I* that produces inputs to the *TCA cycle* (fumarate and pyruvate) were not grouped in the same *TCA* community. Closer inspection of the training data indicated that these pathways appear together in 250 organismal genomes altering the statistical association of pathway occurrences in the network. In this light, pathway communities reflect less the MetaCyc pathway ontology and more the statistical properties of the network itself. This aspect of triUMPF can be leveraged to improve pathway prediction outcomes.

To demonstrate this, we compared pathways predicted for the T1 gold standard *E. coli* K-12 substr. MG1655 (TAX-511145) using Pathologic and triUMPF. Supp. Fig.4a shows the results, where both methods inferred 202 true-positive pathways (green-colored) in common out of 307 expected true-positive pathways (using EcoCyc as a common frame of reference). In addition, Pathologic uniquely predicted 39 (magenta-colored) true-positive pathways while triUMPF uniquely predicted 16 true-positives (purple-colored). This difference arises from the use of taxonomic pruning in Pathologic which improves the recovery of taxonomically constrained pathways and limits false-positive identification. With taxonomic pruning enabled, Pathologic inferred 79 false-positive pathways, and over 170 when pruning was disabled. In contrast triUMPF which does not use taxonomic feature information inferred 84 false-positive pathways. This improvement over Pathologic with pruning disabled reinforces the idea that pathway communities improve the precision of pathway prediction with limited impact on overall recall. Based on these results it is conceivable to train triUMPF on subsets of organismal genomes resulting in more constrained pathway communities for pangenome analysis. For more information on how community properties impact triUMPF performance see Supp. Section 6.

To evaluate triUMPF performance on closely related organismal genomes, we performed pathway prediction on *E. coli* str. CFT073 (TAX-199310), and *E. coli* O157:H7 str. EDL933 (TAX-155864) and compared results to the *E. coli* K-12 reference strain ([31]). Both CFT073 and EDL933 are pathogens infecting the human urinary and gastrointestinal tracts, respectively. Previously, Welch and colleagues described extensive genomic mosaicism between these strains and K-12, defining a core backbone of conserved metabolic genes interspersed with genomic islands encoding common pathogenic or niche defining traits ([31]). Neither CFT073 nor EDL933 genomes are represented in the BioCyc collection of organismal pathway genome databases. A total of 335 and 319 unique pathways were predicted by PathoLogic and triUMPF, respectively. The resulting pathway lists were used to perform a set-difference analysis with K-12 (Fig. 4). Both methods predicted more than 200 pathways encoded by all three strains including core pathways like the *TCA cycle* (Supp. Fig. 4). CFT073 and EDL933 were predicted to share a single common pathway (*TCA cycle IV (2-oxoglutarate decarboxylase)*) by triUMPF. However this pathway variant has not been previously identified in *E. coli* and is likely a false-positive prediction based on known taxonomic range. Both Pathologic and triUMPF predicted the *aerobactin biosynthesis* pathway involved in siderophore production in CFT073

consistent with previous observations ([31]). Similarly, four pathways (e.g. *L-isoleucine biosynthesis III* and *GDP-D-perosamine biosynthesis*) unique to EDL933 were inferred by both methods.

Given the lack of cross validation standards for CFT073 and EDL933 we were unable to determine which method inferred fewer false-positive pathways across the complete set of predicted pathways. Therefore, to constrain this problem on a subset of the data, we applied GapMind ([24]) to analyze amino acid biosynthetic pathways encoded in the genomes of the K-12, CFT073 and EDL933 strains. GapMind is a web-based application developed for annotating amino acid biosynthetic pathways in prokaryotic microorganisms (bacteria and archaea) where each reconstructed pathway is supported by a confidence level. After excluding pathways that were not incorporated in the training set a total of 102 pathways were identified across the three strains encompassing 18 amino acid biosynthetic pathways and 27 pathway variants with high confidence (Supp. Table 3). PathoLogic inferred 49 pathways identified across the three strains encompassing 15 amino acid biosynthetic pathways and 17 pathway variants while triUMPF inferred 51 pathways identified across the three strains encompassing 16 amino acid biosynthetic pathways and 19 pathway variants including *L-methionine biosynthesis* in K-12, CFT073 and EDL933 that was not predicted by PathoLogic. Neither method was able to predict *L-tyrosine biosynthesis I* (see Supp. Materials).

## 5.4 Metabolic Pathway Prediction

**Experimental setup.** Pathway prediction potential of triUMPF was evaluated using the parameter settings described in Section 4.4. The sensitivity of  $\rho$  was initially determined across a range of values {10, 1, 0.1, 0.01, 0.001, 0.0001} using BioCyc as a training set. triUMPF performance on T1 golden datasets was compared to three additional prediction methods including: i)- **MinPath** version 1.2 ([33]), which uses integer programming to recover a conserved set of pathways from a list of enzymatic reactions; ii)- **PathoLogic** version 21 ([16]), which is a symbolic approach that uses a set of manually curated rules to predict pathways; and iii)- **mLGP**R which uses supervised multi-label classification and rich feature information to predict pathways from a list of enzymatic reactions ([3]). In addition to testing on T1 golden datasets, triUMPF performance was compared to both Pathologic and mLGPR on symbiont ([20]), CAMI low complexity data ([26]), and HOTS multi-organismal datasets ([28]). The following metrics were used to report on performance of pathway prediction algorithms including: *average precision*, *average recall*, *average F1 score (F1)*, and *Hamming loss* as described in ([3]).

**Experimental results.** Supp. Fig. 8 shows the inverse effect in predictive performance on T1 golden datasets when decreasing the  $\rho$  before reaching a performance plateau at  $\rho = 0.001$ . The hyperparameter  $\rho$  in Eq. 3.4 controls the amount of information propagation from  $\mathbf{M}$  to pathway label coefficients  $\Theta$ . This suggests, in practice, lesser constraints should be emphasized on  $\Theta$ , while not neglecting associations between EC numbers and pathways indicated in  $\mathbf{M}$ . Having obtained the optimum value of  $\rho$ , we compared triUMPF performance to that of MinPath, PathoLogic and mLGPR. As shown in Supp. Table 4, triUMPF achieved competitive performance against the other methods in terms of average precision with optimal performance on EcoCyc (0.8662). However, with respect to average F1 scores, it under-performed on HumanCyc and AraCyc, yielding average F1 scores of 0.4703 and 0.4775, respectively.

To evaluate triUMPF performance on distributed metabolic pathways we used the reduced genomes of the mealybug symbionts *Moranella* (GenBank NC-015735) and *Tremblaya* (GenBank NC-015736) ([20]). Collectively the two symbiont genomes encode intact biosynthetic pathways for 9 essential amino acids. Pathologic, mLGPR, and triUMPF were used to predict pathways on individual symbiont genomes and a composite genome consisting of both, and resulting amino acid biosynthetic pathway distributions were determined as illustrated in Supp. Fig. 9. Both triUMPF and PathoLogic predicted 6 of the expected amino acid biosynthetic pathways on the composite genome while mLGPR predicted 8 pathways. The pathway for phenylalanine biosynthesis (*L-phenylalanine biosynthesis I*) was excluded from analysis because the associated genes were reported to be missing during the ORF prediction process. False positives were predicted for individual symbiont genomes in *Moranella* and *Tremblaya* using both methods although pathway coverage was reduced in relation to the composite genome.

To evaluate triUMPF performance on more complex multi-organismal genomes we used the CAMI low complexity ([26]) and HOTS datasets ([28]) comparing resulting pathway predictions to both Pathologic and mLGPR. For CAMI low complexity triUMPF achieved an average F1 score of 0.5864 in comparison to 0.4866 for mLGPR which is trained with more than 2500 labeled pathways (Supp. Table 5). Similar results were obtained for HOTS (see Supp. Section 7.5). Among a subset of 180 selected water column pathways, PathoLogic and triUMPF predicted a total of 54 and 58 pathways, respectively, while mLGPR inferred 62. From a real world perspective none of the methods predicted pathways for *photosynthesis light reaction* nor *pyruvate fermentation to (S)-acetoin* although both are expected to be prevalent in the water column. Perhaps, the absence of specific ECs associated with these pathway limits rule-based or ML prediction. Indeed, closer inspection revealed that the enzyme *catabolic acetolactate synthase* was missing from the *pyruvate fermentation to (S)-acetoin* pathway, which is an essential rule encoded in PathoLogic and represented as a feature in mLGPR for predicting that pathway. triUMPF failed to detect this pathway due to constraints enforced in the meta-level network interactions.

## 6 Conclusion

In this paper, we describe triUMPF, a novel ML approach for metabolic pathway inference that combines three stages of NMF to capture relationships between enzymes and pathways within a network followed by community detection to extract higher order network structure. First, a Pathway-EC association ( $\mathbf{M}$ ) matrix, obtained from MetaCyc, is decomposed using the NMF technique to learn a constrained form of the pathway and EC factors, capturing the microscopic structure of  $\mathbf{M}$ . Then, we obtain the community structure (or mesoscopic structure) jointly from both the input datasets and two interaction matrices, Pathway-Pathway interaction and EC-EC interaction. Finally, the consensus relationships between the community structure and data, and between the learned factors from  $\mathbf{M}$  and the pathway labels coefficients are exploited to efficiently optimize metabolic pathway parameters.

We evaluated triUMPF performance based using a corpora of experimental datasets manifesting diverse multi-label properties, including manually curated organismal genomes, synthetic microbial communities and low complexity microbial communities, comparing pathway prediction outcomes to other prediction methods including PathoLogic ([16]) and mLGPR ([3]). In the process of benchmarking, we observed that the BioCyc collection suffers from a class imbalance problem ([13]) where some pathways infrequently occur across PGDBs. This results in a significant sensitivity loss on T1 golden data, where triUMPF tended to predict more frequently observed pathways while missing more infrequent pathways. One potential approach to solve this class-imbalance problem is subsampling the most informative PGDBs for training, hence, reducing false-positives ([18]).

Despite the observed class imbalance problem, triUMPF improved pathway prediction precision without the need for taxonomic rules or EC features to constrain metabolic potential. From an ML perspective this is a promising outcome considering that triUMPF was trained on a reduced number of pathways relative to mLGPR. Future development efforts will explore subsampling approaches to improve sensitivity and the use of constrained taxonomic groups for pangenome and multi-organismal genome pathway inference.

## Acknowledgments

We would like to thank Connor Morgan-Lang, Julia Glinos, Kishori Konwar and Aria Hahn for critical feedback during development of triUMPF.

*Funding:* This work was performed under the auspices of Genome Canada, Genome British Columbia, the Natural Science and Engineering Research Council (NSERC) of Canada, and Compute/Calcul Canada. ARB and RM were supported by UBC four-year doctoral fellowships (4YF) administered through the UBC Graduate Program in Bioinformatics.

*Conflict of Interest:* None declared.

## References

- [1] Amos Bairoch. The enzyme database in 2000. *Nucleic acids research*, 28(1):304–305, 2000.
- [2] Abdur Rahman MA Basher and Steven J Hallam. Leveraging heterogeneous network embedding for metabolic pathway prediction. *bioRxiv*, feb 2020.
- [3] Abdur Rahman MA Basher, Ryan J McLaughlin, and Steven J Hallam. Metabolic pathway inference using multi-label classification with rich pathway features. *bioRxiv*, February 2020.
- [4] Rasmus Bro and Age K Smilde. Principal component analysis. *Analytical Methods*, 6(9):2812–2831, 2014.
- [5] Pablo Carbonell, Jerry Wong, Neil Swainston, Eriko Takano, Nicholas J Turner, Nigel S Scrutton, Douglas B Kell, Rainer Breitling, and Jean-Loup Faulon. Selenzyme: Enzyme selection tool for pathway design. *Bioinformatics*, 34(12):2153–2154, 2018.
- [6] Ron Caspi, Richard Billington, Hartmut Foerster, Carol A Fulcher, Ingrid Keseler, Anamika Kothari, Markus Krummenacker, Mario Latendresse, Lukas A Mueller, Quang Ong, et al. Biocyc: Online resource for genome and metabolic pathway analysis. *The FASEB Journal*, 30(1 Supplement):lb192–lb192, 2016.
- [7] Ron Caspi, Richard Billington, Ingrid M Keseler, Anamika Kothari, Markus Krummenacker, Peter E Midford, Wai Kit Ong, Suzanne Paley, Pallavi Subhraveti, and Peter D Karp. The metacyc database of metabolic pathways and enzymes—a 2019 update. *Nucleic acids research*, 2019.
- [8] Joseph M Dale, Liviu Popescu, and Peter D Karp. Machine learning methods for metabolic pathway prediction. *BMC bioinformatics*, 11(1):1, 2010.
- [9] Santo Fortunato and Darko Hric. Community detection in networks: A user guide. *Physics reports*, 659:1–44, 2016.
- [10] Xiao Fu, Kejun Huang, Nicholas D Sidiropoulos, and Wing-Kin Ma. Nonnegative matrix factorization for signal and data analytics: Identifiability, algorithms, and applications. *arXiv preprint arXiv:1803.01257*, 2018.

- [11] Aria S Hahn, Kishori M Konwar, Stilianos Louca, Niels W Hanson, and Steven J Hallam. The information science of microbial ecology. *Current opinion in microbiology*, 31:209–216, 2016.
- [12] Niels W Hanson, Kishori M Konwar, Alyse K Hawley, Tomer Altman, Peter D Karp, and Steven J Hallam. Metabolic pathways for the whole community. *BMC genomics*, 15(1):1, 2014.
- [13] Haibo He and Edwardo A Garcia. Learning from imbalanced data. *IEEE Transactions on knowledge and data engineering*, 21(9):1263–1284, 2009.
- [14] Dazhi Jiao, Yuzhen Ye, and Haixu Tang. Probabilistic inference of biochemical reactions in microbial communities from metagenomic sequences. *PLoS Comput Biol*, 9(3):e1002981, 2013.
- [15] Minoru Kanehisa, Miho Furumichi, Mao Tanabe, Yoko Sato, and Kanae Morishima. Kegg: new perspectives on genomes, pathways, diseases and drugs. *Nucleic Acids Research*, 45(D1):D353–D361, 2017.
- [16] Peter D Karp, Mario Latendresse, Suzanne M Paley, Markus Krummenacker, Quang D Ong, Richard Billington, Anamika Kothari, Daniel Weaver, Thomas Lee, Pallavi Subhraveti, et al. Pathway tools version 19.0 update: software for pathway/genome informatics and systems biology. *Briefings in bioinformatics*, 17(5):877–890, 2016.
- [17] Kishori M Konwar, Niels W Hanson, Antoine P Pagé, and Steven J Hallam. Metapathways: a modular pipeline for constructing pathway/genome databases from environmental sequence information. *BMC bioinformatics*, 14(1):202, 2013.
- [18] Balaji Lakshminarayanan, Alexander Pritzel, and Charles Blundell. Simple and scalable predictive uncertainty estimation using deep ensembles. In *Advances in Neural Information Processing Systems*, pp. 6402–6413, 2017.
- [19] Yu Li, Ying Wang, Tingting Zhang, Jiawei Zhang, and Yi Chang. Learning network embedding with community structural information. In *Proceedings of the Twenty-Eighth International Joint Conference on Artificial Intelligence, IJCAI-19*, pp. 2937–2943. International Joint Conferences on Artificial Intelligence Organization, 7 2019.
- [20] John P McCutcheon and Carol D Von Dohlen. An interdependent metabolic patchwork in the nested symbiosis of mealybugs. *Current Biology*, 21(16):1366–1372, 2011.
- [21] Andrew G McDonald, Sinead Boyce, and Keith F Tipton. Explorenz: the primary source of the iubmb enzyme list. *Nucleic acids research*, 37(suppl 1):D593–D597, 2009.
- [22] Nagarajan Natarajan and Inderjit S Dhillon. Inductive matrix completion for predicting gene–disease associations. *Bioinformatics*, 30(12):i60–i68, 2014.
- [23] Zoltán N Oltvai and Albert-László Barabási. Life’s complexity pyramid. *Science*, 298(5594):763–764, 2002.
- [24] Morgan N Price, Grant M Zane, Jennifer V Kuehl, Ryan A Melnyk, Judy D Wall, Adam M Deutschbauer, and Adam P Arkin. Filling gaps in bacterial amino acid biosynthesis pathways with high-throughput genetics. *PLoS genetics*, 14(1), 2018.
- [25] Ryan A Rossi, Di Jin, Sungchul Kim, Nesreen K Ahmed, Danai Koutra, and John Boaz Lee. From community to role-based graph embeddings. *arXiv preprint arXiv:1908.08572*, 2019.
- [26] Alexander Sczyrba, Peter Hofmann, Peter Belmann, David Koslicki, Stefan Janssen, Johannes Dröge, Ivan Gregor, Stephan Majda, Jessika Fiedler, Eik Dahms, et al. Critical assessment of metagenome interpretation—a benchmark of metagenomics software. *Nature methods*, 14(11):1063, 2017.
- [27] Mahdi Shafiei, Katherine A Dunn, Hugh Chipman, Hong Gu, and Joseph P Bielawski. Biomenet: A bayesian model for inference of metabolic divergence among microbial communities. *PLoS Comput Biol*, 10(11):e1003918, 2014.
- [28] Frank J Stewart, Adrian K Sharma, Jessica A Bryant, John M Eppley, and Edward F DeLong. Community transcriptomics reveals universal patterns of protein sequence conservation in natural microbial communities. *Genome biology*, 12(3):R26, 2011.
- [29] David Toubiana, Rami Puzis, Lingling Wen, Noga Sikron, Assylay Kurmanbayeva, Aigerim Soltabayeva, Maria del Mar Rubio Wilhelmi, Nir Sade, Aaron Fait, Moshe Sagi, et al. Combined network analysis and machine learning allows the prediction of metabolic pathways from tomato metabolomics data. *Communications Biology*, 2(1):214, 2019.
- [30] Xiao Wang, Peng Cui, Jing Wang, Jian Pei, Wenwu Zhu, and Shiqiang Yang. Community preserving network embedding. In *Thirty-First AAAI Conference on Artificial Intelligence*, 2017.
- [31] Rodney A Welch, V Burland, GIII Plunkett, P Redford, P Roesch, D Rasko, EL Buckles, S-R Liou, A Boutin, Jeremiah Hackett, et al. Extensive mosaic structure revealed by the complete genome sequence of uropathogenic escherichia coli. *Proceedings of the National Academy of Sciences*, 99(26):17020–17024, 2002.
- [32] Zi Yang and George Michailidis. A non-negative matrix factorization method for detecting modules in heterogeneous omics multi-modal data. *Bioinformatics*, 32(1):1–8, 2015.
- [33] Yuzhen Ye and Thomas G Doak. A parsimony approach to biological pathway reconstruction/inference for genomes and metagenomes. *PLoS Comput Biol*, 5(8):e1000465, 2009.

# Supplementary - Metabolic pathway inference using non-negative matrix factorization with community detection

Abdur Rahman M. A. Basher, Ryan J. McLaughlin, and Steven J. Hallam

May 27, 2020

Here, we provide additional terminologies (Section 1) the analytical expression of each individual triUMPF parameters (Section 2). We then describe the characteristics of different datasets used in testing (Section 3). Finally, additional experimental results, including adding EC features, network reconstruction and visualization, and pathway prediction, are provided (Sections 4, 5, 6, & 7). Consult the primary text for the symbol definitions and the problem formulation.

## 1 Definitions

Here, we formulate three graphs, one representing associations between pathways and enzymes indicated by enzyme commission (EC) numbers, one representing interactions between enzymes and another representing interactions between pathways.

**Definition 1.1. Pathway-EC Association (P2E).** Let  $\mathcal{G}'^{(\text{path})} = \{\mathcal{E}, \mathcal{Z}^{(r)}\}$  be a subgraph of  $\mathcal{G}^{(\text{path})}$ , such that  $\mathcal{E} \subset \mathcal{R}$  with  $r \ll r'$  enzymatic reactions. Then, the Pathway-EC association is defined as a matrix  $\mathbf{M} \in \mathbb{Z}_{\geq 0}^{t \times r}$ , where each row corresponds to a pathway, and each column represent an EC, such that  $\mathbf{M}_{i,j} \geq 1$  if an EC  $j$  is in pathway  $i$  and 0 otherwise. ■

Typically, the association matrix  $\mathbf{M}$  is extremely sparse. Using reaction and pathway graph topology, we build interaction adjacency matrices as follows.

**Definition 1.2. EC-EC Interaction (E2E).** Given  $\mathcal{G}'^{(\text{rxn})} \subset \mathcal{G}^{(\text{rxn})}$ , we define an EC-EC interaction matrix  $\mathbf{B} \in \mathbb{Z}_{\geq 0}^{r \times r}$  such that an entry  $\mathbf{B}_{i,j}$  is a binary value encoding an interaction between two ECs  $i$  and  $j$  iff they both share a compound, i.e.,  $\Omega_{i,k}^{(c)} \wedge \Omega_{j,k}^{(c)} = 1$  where  $k \in \mathcal{C}$ . ■

**Definition 1.3. Pathway-Pathway Interaction (P2P).** Given  $\mathcal{G}^{(\text{path})}$ , we define a Pathway-Pathway interaction matrix  $\mathbf{A} \in \mathbb{Z}_{\geq 0}^{t \times t}$  such that an entry  $\mathbf{A}_{i,j}$  is a binary value indicating an interaction between pathways  $i$  and  $j$  iff there exists a reaction  $k \in \mathcal{R}$  where it's associated compounds are either substrate or product in both  $i$  and  $j$  pathways. ■

## 2 Optimization Algorithm Derivation

In this section, we derive the optimization for triUMPF's objective function:

$$\mathcal{J} = \mathcal{J}^{\text{fact}}(\mathbf{W}, \mathbf{H}, \mathbf{U}, \mathbf{V}) + \mathcal{J}^{\text{comm}}(\mathbf{C}, \mathbf{K}) + \mathcal{J}^{\text{path}}(\mathbf{T}, \mathbf{R}, \Theta, \mathbf{Z}, \mathbf{L}) \quad (2.1)$$

where,

$$\begin{aligned} \mathcal{J}^{\text{fact}}(\mathbf{W}, \mathbf{H}, \mathbf{U}, \mathbf{V}) &= \min_{\mathbf{W}, \mathbf{H}, \mathbf{U}, \mathbf{V}} \|\mathbf{M} - \mathbf{W}\mathbf{H}^\top\|_F^2 + \lambda_1 \|\mathbf{W} - \mathbf{P}\mathbf{U}\|_F^2 + \lambda_2 \|\mathbf{H} - \mathbf{E}\mathbf{V}\|_F^2 \\ &\quad + \lambda_3 \|\mathbf{U} - \mathbf{V}\|_F^2 + \lambda_4 (\|\mathbf{W}\|_F^2 + \|\mathbf{H}\|_F^2 + \|\mathbf{U}\|_F^2 + \|\mathbf{V}\|_F^2) \\ &\text{s.t. } \{\mathbf{W}, \mathbf{H}, \mathbf{U}, \mathbf{V}\} \geq 0 \\ \mathcal{J}^{\text{comm}}(\mathbf{C}, \mathbf{K}) &= \min_{\mathbf{C}, \mathbf{K}} \|\mathbf{A}^{\text{prox}} - \mathbf{P}\mathbf{T}\mathbf{C}^\top\|_F^2 + \|\mathbf{B}^{\text{prox}} - \mathbf{E}\mathbf{R}\mathbf{K}^\top\|_F^2 + \alpha \|\mathbf{C}^\top\mathbf{C} - \mathbf{I}\|_F^2 \\ &\quad + \beta \|\mathbf{K}^\top\mathbf{K} - \mathbf{I}\|_F^2 + \lambda_5 (\|\mathbf{C}\|_F^2 + \|\mathbf{K}\|_F^2) \\ &\text{s.t. } \{\mathbf{C}, \mathbf{K}\} \geq 0 \\ \mathcal{J}^{\text{path}}(\mathbf{T}, \mathbf{R}, \Theta, \mathbf{L}, \mathbf{Z}) &= \min_{\mathbf{T}, \mathbf{R}, \Theta, \mathbf{L}, \mathbf{Z}} \sum_{i \in n} \sum_{k \in t} \log \left( 1 + e^{-\mathbf{y}_k^{(i)} \Theta_k \mathbf{x}^{(i)}} \right) + \|\mathbf{X} - \mathbf{L}\mathbf{R}\mathbf{K}^\top\|_F^2 \\ &\quad + \|\mathbf{Y} - \mathbf{L}\mathbf{T}\mathbf{C}^\top\|_F^2 + \rho \|\Theta - \mathbf{Z}\mathbf{H}\mathbf{W}^\top\|_F^2 + \lambda_5 (\|\mathbf{T}\|_F^2 + \|\mathbf{R}\|_F^2) \\ &\quad + \lambda_6 (\|\Theta\|_{2,1} + \|\mathbf{L}\|_F^2 + \|\mathbf{Z}\|_F^2) \\ &\text{s.t. } \{\mathbf{T}, \mathbf{R}\} \geq 0 \end{aligned} \quad (2.2)$$

where  $\mathbf{M} \in \mathbb{Z}_{\geq 0}^{t \times r}$  is the Pathway-EC association matrix,  $\mathbf{W} \in \mathbb{R}^{t \times k}$  stores the latent factors for pathways, and  $\mathbf{H} \in \mathbb{R}^{r \times k}$ , known as the basis matrix, can be thought of as latent factors associated with ECs. The pathway and EC features are represented by  $\mathbf{P} \in \mathbb{R}^{t \times m}$  and  $\mathbf{E} \in \mathbb{R}^{r \times m}$ , respectively. Both  $\mathbf{U} \in \mathbb{R}^{m \times k}$  and  $\mathbf{V} \in \mathbb{R}^{m \times k}$  are linear transformation matrices.  $\mathbf{A}^{\text{prox}} \in \mathbb{Z}_{\geq 0}^{t \times t}$  and  $\mathbf{B}^{\text{prox}} \in \mathbb{Z}_{\geq 0}^{r \times r}$  are two higher order Pathway-Pathway and EC-EC interaction matrices. The pathway and EC community representation matrices are denoted by  $\mathbf{T} \in \mathbb{R}^{m \times p}$  and  $\mathbf{R} \in \mathbb{R}^{m \times v}$ , respectively, while their associated community indicator matrices are symbolized as  $\mathbf{C} \in \mathbb{R}^{t \times p}$  and  $\mathbf{K} \in \mathbb{R}^{r \times v}$ , respectively.  $\mathbf{L} \in \mathbb{R}^{n \times m}$  and  $\mathbf{Z} \in \mathbb{R}^{r \times r}$  are the two auxiliary matrices and  $\Theta \in \mathbb{R}^{t \times r}$  is the weight matrix.

The objective function in Eq. 2.2 is non-convex due to multiple non-negative constraints. Numerous algorithms have been proposed to optimize the objective function, including alternating non-negative least squares [7] and hierarchical alternating least squares [3]. Here, we employ the original algorithm for NMF which was introduced in [9] and consists of simple multiplicative update rules (with auxiliary variables) that are based on the gradient descent technique [5]. Beginning with random positive initialization, element-wise updates of Eq 2.1 w.r.t  $\mathbf{W}, \mathbf{H}, \mathbf{U}, \mathbf{V}, \mathbf{C}, \mathbf{K}, \mathbf{T}, \mathbf{R}, \Theta, \mathbf{Z}$ , and  $\mathbf{L}$  at each iteration are applied until convergence. The gradient descent aims to search for a local minima of the cost function by moving in the direction of its steepest descent. By introducing Lagrangian multipliers (auxiliary variables), which are  $\psi, \phi, \varphi, \varrho, \zeta, \varpi, \kappa$ , and  $\xi$  to enforce the constraints for  $\mathbf{W}, \mathbf{H}, \mathbf{U}, \mathbf{V}, \mathbf{C}, \mathbf{T}, \mathbf{R}, \mathbf{K}$ , respectively, Eq. 2.2 can be reformulated as:

$$\begin{aligned} \mathcal{J}^{\text{fact}}(\mathbf{W}, \mathbf{H}, \mathbf{U}, \mathbf{V}) &= \min_{\mathbf{W}, \mathbf{H}, \mathbf{U}, \mathbf{V}} \text{tr} \left( (\mathbf{M} - \mathbf{W}\mathbf{H}^\top)^\top (\mathbf{M} - \mathbf{W}\mathbf{H}^\top) \right) \\ &\quad + \lambda_1 \text{tr} \left( (\mathbf{W} - \mathbf{P}\mathbf{U})^\top (\mathbf{W} - \mathbf{P}\mathbf{U}) \right) + \lambda_2 \text{tr} \left( (\mathbf{H} - \mathbf{E}\mathbf{V})^\top (\mathbf{H} - \mathbf{E}\mathbf{V}) \right) \\ &\quad + \lambda_3 \text{tr} \left( (\mathbf{U} - \mathbf{V})^\top (\mathbf{U} - \mathbf{V}) \right) \\ &\quad + \lambda_4 \left( \text{tr}(\mathbf{W}^\top\mathbf{W}) + \text{tr}(\mathbf{H}^\top\mathbf{H}) + \text{tr}(\mathbf{U}^\top\mathbf{U}) + \text{tr}(\mathbf{V}^\top\mathbf{V}) \right) \\ &\quad + \text{tr}(\psi\mathbf{W}) + \text{tr}(\phi\mathbf{H}) + \text{tr}(\varphi\mathbf{U}) + \text{tr}(\varrho\mathbf{V}) \end{aligned} \quad (2.3)$$

$$\begin{aligned} \mathcal{J}^{\text{comm}}(\mathbf{C}, \mathbf{K}) &= \min_{\mathbf{C}, \mathbf{K}} \text{tr} \left( (\mathbf{A}^{\text{prox}} - \mathbf{P}\mathbf{T}\mathbf{C}^\top)^\top (\mathbf{A}^{\text{prox}} - \mathbf{P}\mathbf{T}\mathbf{C}^\top) \right) \\ &\quad + \text{tr} \left( (\mathbf{B}^{\text{prox}} - \mathbf{E}\mathbf{R}\mathbf{K}^\top)^\top (\mathbf{B}^{\text{prox}} - \mathbf{E}\mathbf{R}\mathbf{K}^\top) \right) \\ &\quad + \alpha \text{tr} \left( (\mathbf{C}^\top\mathbf{C} - \mathbf{I})^\top (\mathbf{C}^\top\mathbf{C} - \mathbf{I}) \right) + \beta \text{tr} \left( (\mathbf{K}^\top\mathbf{K} - \mathbf{I})^\top (\mathbf{K}^\top\mathbf{K} - \mathbf{I}) \right) \\ &\quad + \lambda_5 \left( \text{tr}(\mathbf{C}^\top\mathbf{C}) + \text{tr}(\mathbf{K}^\top\mathbf{K}) \right) + \text{tr}(\varpi\mathbf{C}) + \text{tr}(\xi\mathbf{K}) \end{aligned} \quad (2.4)$$

$$\begin{aligned}
\mathcal{J}^{\text{path}}(\mathbf{T}, \mathbf{R}, \Theta, \mathbf{L}, \mathbf{Z}) = & \min_{\mathbf{T}, \mathbf{R}, \Theta, \mathbf{L}, \mathbf{Z}} \sum_{i \in n} \sum_{k \in t} \log \left( 1 + e^{-y_k^{(i)} \Theta_k^\top \mathbf{x}^{(i)}} \right) \\
& + \text{tr} \left( (\mathbf{X} - \mathbf{L}\mathbf{R}\mathbf{K}^\top)^\top (\mathbf{X} - \mathbf{L}\mathbf{R}\mathbf{K}^\top) \right) + \text{tr} \left( (\mathbf{Y} - \mathbf{L}\mathbf{T}\mathbf{C}^\top)^\top (\mathbf{Y} - \mathbf{L}\mathbf{T}\mathbf{C}^\top) \right) \\
& + \rho \text{tr} \left( (\Theta - \mathbf{Z}\mathbf{H}\mathbf{W}^\top)^\top (\Theta - \mathbf{Z}\mathbf{H}\mathbf{W}^\top) \right) + \lambda_5 \left( \text{tr}(\mathbf{T}^\top \mathbf{T}) + \text{tr}(\mathbf{R}^\top \mathbf{R}) \right) \\
& + \lambda_6 \left( \|\Theta\|_{2,1} + \text{tr}(\mathbf{L}^\top \mathbf{L}) + \text{tr}(\mathbf{Z}^\top \mathbf{Z}) \right) + \text{tr}(\zeta \mathbf{T}) + \text{tr}(\kappa \mathbf{R})
\end{aligned} \tag{2.5}$$

where  $\text{tr}(\cdot)$  denotes the trace of a matrix. Using the addition property of the transpose,  $(\mathbf{X} + \mathbf{Y})^\top = \mathbf{X}^\top + \mathbf{Y}^\top$ , and its multiplication property,  $(\mathbf{X}\mathbf{Y})^\top = \mathbf{Y}^\top \mathbf{X}^\top$ , we can expand the trace of the first term as

$$\text{tr} \left( (\mathbf{M} - \mathbf{W}\mathbf{H}^\top)^\top (\mathbf{M} - \mathbf{W}\mathbf{H}^\top) \right) = \text{tr} \left( \mathbf{M}^\top \mathbf{M} - \mathbf{M}^\top \mathbf{W}\mathbf{H}^\top - \mathbf{W}^\top \mathbf{H}\mathbf{M} + \mathbf{H}\mathbf{W}^\top \mathbf{W}\mathbf{H}^\top \right) \tag{2.6}$$

By expanding the remaining terms in Eq. 2.3 and using the trace of a sum of matrix property,  $\text{tr}(\mathbf{X} + \mathbf{Y}) = \text{tr}(\mathbf{X}) + \text{tr}(\mathbf{Y})$ , we obtain the following formula:

$$\begin{aligned}
\mathcal{J}^{\text{fact}}(\mathbf{W}, \mathbf{H}, \mathbf{U}, \mathbf{V}) = & \min_{\mathbf{W}, \mathbf{H}, \mathbf{U}, \mathbf{V}} \text{tr}(\mathbf{M}^\top \mathbf{M}) - \text{tr}(\mathbf{M}^\top \mathbf{W}\mathbf{H}^\top) - \text{tr}(\mathbf{W}^\top \mathbf{H}\mathbf{M}) + \text{tr}(\mathbf{H}\mathbf{W}^\top \mathbf{W}\mathbf{H}^\top) \\
& + \lambda_1 \left( \text{tr}(\mathbf{W}^\top \mathbf{W}) - \text{tr}(\mathbf{W}^\top \mathbf{P}\mathbf{U}) - \text{tr}(\mathbf{U}^\top \mathbf{P}^\top \mathbf{W}) + \text{tr}(\mathbf{U}^\top \mathbf{P}^\top \mathbf{P}\mathbf{U}) \right) \\
& + \lambda_2 \left( \text{tr}(\mathbf{H}^\top \mathbf{H}) - \text{tr}(\mathbf{H}^\top \mathbf{E}\mathbf{V}) - \text{tr}(\mathbf{V}^\top \mathbf{E}^\top \mathbf{H}) + \text{tr}(\mathbf{V}^\top \mathbf{E}^\top \mathbf{E}\mathbf{V}) \right) \\
& + \lambda_3 \left( \text{tr}(\mathbf{U}^\top \mathbf{U}) - 2\text{tr}(\mathbf{U}^\top \mathbf{V}) + \text{tr}(\mathbf{V}^\top \mathbf{V}) \right) \\
& + \lambda_4 \left( \text{tr}(\mathbf{W}^\top \mathbf{W}) + \text{tr}(\mathbf{H}^\top \mathbf{H}) + \text{tr}(\mathbf{U}^\top \mathbf{U}) + \text{tr}(\mathbf{V}^\top \mathbf{V}) \right) \\
& + \text{tr}(\psi \mathbf{W}) + \text{tr}(\phi \mathbf{H}) + \text{tr}(\varphi \mathbf{U}) + \text{tr}(\varrho \mathbf{V})
\end{aligned} \tag{2.7}$$

Similar to the process of getting Eq. 2.7, we expand the Eq. 2.4 as:

$$\begin{aligned}
\mathcal{J}^{\text{comm}}(\mathbf{C}, \mathbf{K}) = & \min_{\mathbf{C}, \mathbf{K}} \text{tr}(\mathbf{A}^{\text{prox}\top} \mathbf{A}^{\text{prox}}) - \text{tr}(\mathbf{A}^{\text{prox}\top} \mathbf{P}\mathbf{T}\mathbf{C}^\top) - \text{tr}(\mathbf{C}\mathbf{T}^\top \mathbf{P}^\top \mathbf{A}^{\text{prox}}) + \text{tr}(\mathbf{C}\mathbf{T}^\top \mathbf{P}^\top \mathbf{P}\mathbf{T}\mathbf{C}^\top) \\
& + \text{tr}(\mathbf{B}^{\text{prox}\top} \mathbf{B}^{\text{prox}}) - \text{tr}(\mathbf{B}^{\text{prox}\top} \mathbf{E}\mathbf{R}\mathbf{K}^\top) - \text{tr}(\mathbf{K}\mathbf{R}^\top \mathbf{E}^\top \mathbf{B}^{\text{prox}}) + \text{tr}(\mathbf{K}\mathbf{R}^\top \mathbf{E}^\top \mathbf{E}\mathbf{R}\mathbf{K}^\top) \\
& + \alpha \left( \text{tr}(\mathbf{C}^\top \mathbf{C}\mathbf{C}^\top \mathbf{C}) - 2\text{tr}(\mathbf{C}^\top \mathbf{C}) + t \right) + \beta \left( \text{tr}(\mathbf{K}^\top \mathbf{K}\mathbf{K}^\top \mathbf{K}) - 2\text{tr}(\mathbf{K}^\top \mathbf{K}) + r \right) \\
& + \lambda_5 \left( \text{tr}(\mathbf{C}^\top \mathbf{C}) + \text{tr}(\mathbf{K}^\top \mathbf{K}) \right) + \text{tr}(\varpi \mathbf{C}) + \text{tr}(\xi \mathbf{K})
\end{aligned} \tag{2.8}$$

Expand the Eq. 2.5, we obtain the following:

$$\begin{aligned}
\mathcal{J}^{\text{path}}(\mathbf{T}, \mathbf{R}, \Theta, \mathbf{L}, \mathbf{Z}) = & \min_{\mathbf{T}, \mathbf{R}, \Theta, \mathbf{L}, \mathbf{Z}} \sum_{i \in n} \sum_{k \in t} \log \left( 1 + e^{-y_k^{(i)} \Theta_k^\top \mathbf{x}^{(i)}} \right) \\
& + \text{tr}(\mathbf{X}^\top \mathbf{X}) - \text{tr}(\mathbf{X}^\top \mathbf{L}\mathbf{R}\mathbf{K}^\top) - \text{tr}(\mathbf{K}\mathbf{R}^\top \mathbf{L}^\top \mathbf{X}) + \text{tr}(\mathbf{K}\mathbf{R}^\top \mathbf{L}^\top \mathbf{L}\mathbf{R}\mathbf{K}^\top) \\
& + \text{tr}(\mathbf{Y}^\top \mathbf{Y}) - \text{tr}(\mathbf{Y}^\top \mathbf{L}\mathbf{T}\mathbf{C}^\top) - \text{tr}(\mathbf{C}\mathbf{T}^\top \mathbf{L}^\top \mathbf{Y}) + \text{tr}(\mathbf{C}\mathbf{T}^\top \mathbf{L}^\top \mathbf{L}\mathbf{T}\mathbf{C}^\top) \\
& + \rho \left( \text{tr}(\Theta^\top \Theta) - \text{tr}(\Theta^\top \mathbf{Z}\mathbf{H}\mathbf{W}^\top) - \text{tr}(\mathbf{W}\mathbf{H}^\top \mathbf{Z}^\top \Theta) + \text{tr}(\mathbf{W}\mathbf{H}^\top \mathbf{Z}^\top \mathbf{Z}\mathbf{H}\mathbf{W}^\top) \right) \\
& + \lambda_5 \left( \text{tr}(\mathbf{T}^\top \mathbf{T}) + \text{tr}(\mathbf{R}^\top \mathbf{R}) \right) + \lambda_6 \left( \|\Theta\|_{2,1} + \text{tr}(\mathbf{L}^\top \mathbf{L}) + \text{tr}(\mathbf{Z}^\top \mathbf{Z}) \right) \\
& + \text{tr}(\zeta \mathbf{T}) + \text{tr}(\kappa \mathbf{R})
\end{aligned} \tag{2.9}$$

As explained earlier, the objective functions in Eqs 2.7, 2.8, and 2.9, are not convex with respect to all parameters combined. Instead in NMF,  $\mathbf{W}$ ,  $\mathbf{H}$ ,  $\mathbf{U}$ ,  $\mathbf{V}$ ,  $\mathbf{C}$ ,  $\mathbf{K}$ ,  $\mathbf{T}$ ,  $\mathbf{R}$ ,  $\Theta$ ,  $\mathbf{L}$ , and  $\mathbf{Z}$  are individually optimized in an iterative process, where we update one matrix at a time while keeping the remaining matrices fixed. This ensures that each subproblem converges to the local minima. This method is called *block-coordinate descent*. Hence, the update of parameters occur in the following four alternate optimization steps for  $\mathcal{J}^{\text{fact}}$ : i)- the basis matrix  $\mathbf{W}$ , representing pathway factors, ii)- the latent coefficient matrix  $\mathbf{H}$ , representing EC factors, iii)- the linear transformation  $\mathbf{U}$ , and iv)- the other linear transformation  $\mathbf{V}$ . For  $\mathcal{J}^{\text{comm}}$ , we alternate between the community indicator matrix  $\mathbf{C}$  for pathways and the other community indicator matrix  $\mathbf{K}$  for ECs. Finally, we optimize, alternatively, the two community representation matrices  $\mathbf{T}$  and  $\mathbf{R}$  for pathways and ECs, respectively, the two auxiliary matrices  $\mathbf{L}$  and  $\mathbf{Z}$ , and the input weight matrix  $\Theta$ . The three sub-objective functions,  $\mathcal{J}^{\text{fact}}$ ,  $\mathcal{J}^{\text{comm}}$ , and  $\mathcal{J}^{\text{path}}$  are run simultaneously in a divide and conquer strategy. Detailed rules for updating all the variables are outlined below.

1. **Update the basis matrix  $\mathbf{W}$ .** To update the feature matrix  $\mathbf{W}$ , we fix  $\mathbf{H}$ ,  $\mathbf{U}$  and  $\mathbf{V}$ . Then, the objective function in Eq. 2.7 w.r.t  $\mathbf{W}$  is reduced to, after dropping min for brevity:

$$\begin{aligned} \mathcal{J}^{\text{fact}}(\mathbf{W}) = & -\text{tr}(\mathbf{M}^\top \mathbf{W} \mathbf{H}^\top) - \text{tr}(\mathbf{W}^\top \mathbf{H} \mathbf{M}) + \text{tr}(\mathbf{H} \mathbf{W}^\top \mathbf{W} \mathbf{H}^\top) \\ & + \lambda_1 \left( \text{tr}(\mathbf{W}^\top \mathbf{W}) - \text{tr}(\mathbf{W}^\top \mathbf{P} \mathbf{U}) - \text{tr}(\mathbf{U}^\top \mathbf{P}^\top \mathbf{W}) \right) + \lambda_4 \text{tr}(\mathbf{W}^\top \mathbf{W}) + \text{tr}(\psi \mathbf{W}) \end{aligned} \quad (2.10)$$

where  $\psi$  is the Lagrange multiplier for the constraint  $\mathbf{W} \geq 0$ . For computing the gradient of this equation, we use the following properties with respect to  $\mathbf{X}$ :

$$\begin{aligned} \nabla_{\mathbf{X}} \text{tr}(\mathbf{X}^\top \mathbf{X}) &= 2\mathbf{X} \\ \nabla_{\mathbf{X}} \text{tr}(\mathbf{X} \mathbf{Y}) &= \mathbf{Y}^\top \\ \nabla_{\mathbf{X}} \text{tr}(\mathbf{X}^\top \mathbf{Y}) &= \mathbf{Y} \\ \nabla_{\mathbf{X}} \text{tr}(\mathbf{X}^\top \mathbf{Y} \mathbf{X}) &= (\mathbf{Y} + \mathbf{Y}^\top) \mathbf{X} \\ \nabla_{\mathbf{X}} \text{tr}(\mathbf{X} \mathbf{Y} \mathbf{X}^\top) &= \mathbf{X} (\mathbf{Y}^\top + \mathbf{Y}) \\ \nabla_{\mathbf{X}} \text{tr}(\mathbf{Y} \mathbf{X} \mathbf{Z}) &= \mathbf{Y}^\top \mathbf{Z}^\top \\ \nabla_{\mathbf{X}} \text{tr}(\mathbf{Y} \mathbf{X}^\top \mathbf{Z}) &= \mathbf{Z} \mathbf{Y} \end{aligned} \quad (2.11)$$

By computing the gradient of the cost function in Eq. 2.10 w.r.t  $\mathbf{W}$  to 0, we have:

$$\psi = 2\mathbf{M} \mathbf{H} - 2\mathbf{W} (\mathbf{H}^\top \mathbf{H} + Q) + 2\lambda_1 \mathbf{P} \mathbf{U} \quad (2.12)$$

where  $Q = (\lambda_1 + \lambda_4)$ . Following the Karush-Kuhn-Tucker (KKT) condition for the nonnegativity of  $\mathbf{W}$ , we have the following equation:

$$2 \left( \mathbf{M} \mathbf{H} - \mathbf{W} (\mathbf{H}^\top \mathbf{H} + Q) + \lambda_1 \mathbf{P} \mathbf{U} \right)_{k,j} \mathbf{W}_{j,k} = \psi_{j,k} \mathbf{W}_{j,k} = 0 \quad (2.13)$$

Given an initial value of  $\mathbf{W}$ , the successive updating rule of  $\mathbf{W}$  is:

$$\mathbf{W} \leftarrow \mathbf{W} \circ \frac{\mathbf{M} \mathbf{H} + \lambda_1 \mathbf{P} \mathbf{U}}{\mathbf{W} (\mathbf{H}^\top \mathbf{H} + Q)} \quad (2.14)$$

The iterative update rules in Eq. 2.14 is transformed into multiplicative update rules, which cannot generate negative elements since all values are positive and only multiplications and divisions are involved at each iteration [8].

2. **Update the latent coefficient matrix  $\mathbf{H}$ .** The feature matrix  $\mathbf{H}$  is updates as described above in which  $\mathbf{W}$ ,  $\mathbf{U}$  and  $\mathbf{V}$  are fixed to obtain the objective function for Eq. 2.7 w.r.t  $\mathbf{H}$  as:

$$\begin{aligned} \mathcal{J}^{\text{fact}}(\mathbf{H}) = & -\text{tr}(\mathbf{M}^\top \mathbf{W} \mathbf{H}^\top) - \text{tr}(\mathbf{W}^\top \mathbf{H} \mathbf{M}) + \text{tr}(\mathbf{H} \mathbf{W}^\top \mathbf{W} \mathbf{H}^\top) \\ & + \lambda_1 \left( \text{tr}(\mathbf{H}^\top \mathbf{H}) - \text{tr}(\mathbf{H}^\top \mathbf{E} \mathbf{V}) - \text{tr}(\mathbf{V}^\top \mathbf{E}^\top \mathbf{H}) \right) + \lambda_4 \text{tr}(\mathbf{H}^\top \mathbf{H}) + \text{tr}(\phi \mathbf{H}) \end{aligned} \quad (2.15)$$

Taking the derivative of the cost function in Eq. 2.15 w.r.t  $\mathbf{H}$  to 0 and using the gradient properties in Eq. 2.11, we obtain the following:

$$\phi = 2\mathbf{M}^\top \mathbf{W} - 2\mathbf{H} (\mathbf{W}^\top \mathbf{W} + Q) + 2\lambda_1 \mathbf{E} \mathbf{V} \quad (2.16)$$

where  $Q = (\lambda_1 + \lambda_4)$ . With the KKT complementary condition for the nonnegativity of  $\mathbf{H}$ , we have:

$$2 \left( \mathbf{M}^\top \mathbf{W} - \mathbf{H} (\mathbf{W}^\top \mathbf{W} + Q) + \lambda_1 \mathbf{E} \mathbf{V} \right)_{j,k} \mathbf{H}_{j,k} = \phi_{j,k} \mathbf{H}_{j,k} = 0 \quad (2.17)$$

The multiplicative updates after some algebraic manipulation w.r.t parameter  $\mathbf{H}$ :

$$\mathbf{H} \leftarrow \mathbf{H} \circ \frac{\mathbf{M}^\top \mathbf{W} + \lambda_1 \mathbf{E} \mathbf{V}}{\mathbf{H} (\mathbf{W}^\top \mathbf{W} + Q)} \quad (2.18)$$

3. **Update the linear transformation  $\mathbf{U}$ .** Suppose that  $\mathbf{W}$ ,  $\mathbf{H}$  and  $\mathbf{V}$  are fixed, then Eq. 2.7 w.r.t  $\mathbf{U}$  is reduced to:

$$\begin{aligned} \mathcal{J}^{\text{fact}}(\mathbf{U}) = & \lambda_1 \left( -\text{tr}(\mathbf{W}^\top \mathbf{P} \mathbf{U}) - \text{tr}(\mathbf{U}^\top \mathbf{P}^\top \mathbf{W}) + \text{tr}(\mathbf{U}^\top \mathbf{P}^\top \mathbf{P} \mathbf{U}) \right) \\ & + \lambda_3 \left( \text{tr}(\mathbf{U}^\top \mathbf{U}) - 2\text{tr}(\mathbf{U}^\top \mathbf{V}) \right) + \lambda_4 \text{tr}(\mathbf{U}^\top \mathbf{U}) + \text{tr}(\varphi \mathbf{U}) \end{aligned} \quad (2.19)$$



Then we take the derivative of above formula with respect to the transformation matrix  $\mathbf{U}$  to 0:

$$\varphi = 2\lambda_1 \mathbf{P}^\top \mathbf{W} - 2(\lambda_1 \mathbf{P}^\top \mathbf{P} + D)\mathbf{U} + 2\lambda_3 \mathbf{V} \quad (2.20)$$

where  $D = (\lambda_3 + \lambda_4)$ . Formulating the above equation based on Karush–Kuhn–Tucker conditions for the nonnegativity of  $\mathbf{U}$  results in:

$$2\left(\lambda_1 \mathbf{P}^\top \mathbf{W} - (\lambda_1 \mathbf{P}^\top \mathbf{P} + D)\mathbf{U} + \lambda_3 \mathbf{V}\right)_{j,k} \mathbf{U}_{j,k} = \varphi_{j,k} \mathbf{U}_{j,k} = 0 \quad (2.21)$$

Then, the parameter  $\mathbf{U}$  is updated according to:

$$\mathbf{U} \leftarrow \mathbf{U} \circ \frac{\lambda_1 \mathbf{P}^\top \mathbf{W} + \lambda_3 \mathbf{V}}{(\lambda_1 \mathbf{P}^\top \mathbf{P} + D)\mathbf{U}} \quad (2.22)$$

4. **Update the linear transformation  $\mathbf{V}$ .** To update the linear transformation matrix  $\mathbf{V}$ , that  $\mathbf{W}$ ,  $\mathbf{H}$  and  $\mathbf{U}$  are fixed, then the transformation matrix  $\mathbf{V}$  is updated such that the error is minimized:

$$\begin{aligned} \mathcal{J}^{\text{fact}}(\mathbf{V}) = & \lambda_2 \left( -\text{tr}(\mathbf{H}^\top \mathbf{E} \mathbf{V}) - \text{tr}(\mathbf{V}^\top \mathbf{E}^\top \mathbf{H}) + \text{tr}(\mathbf{V}^\top \mathbf{E}^\top \mathbf{E} \mathbf{V}) \right) \\ & + \lambda_3 \left( -2\text{tr}(\mathbf{U}^\top \mathbf{V}) + \text{tr}(\mathbf{V}^\top \mathbf{V}) \right) + \lambda_4 \text{tr}(\mathbf{V}^\top \mathbf{V}) + \text{tr}(\varrho \mathbf{V}) \end{aligned} \quad (2.23)$$

Taking the derivative of this error with respect to  $\mathbf{V}$  to 0 and after some manipulations, we have:

$$\varrho = 2\lambda_2 \mathbf{E}^\top \mathbf{H} - 2(\lambda_2 \mathbf{E}^\top \mathbf{E} + D)\mathbf{V} + 2\lambda_3 \mathbf{U} \quad (2.24)$$

where  $D = (\lambda_3 + \lambda_4)$ . Following the Karush–Kuhn–Tucker conditions for the nonnegativity of  $\mathbf{V}$ , we have:

$$2\left(\lambda_2 \mathbf{E}^\top \mathbf{H} - (\lambda_2 \mathbf{E}^\top \mathbf{E} + D)\mathbf{V} + \lambda_3 \mathbf{U}\right)_{j,k} \mathbf{V}_{j,k} = \varrho_{j,k} \mathbf{V}_{j,k} = 0 \quad (2.25)$$

As usual, the parameter  $\mathbf{V}$  is updated according:

$$\mathbf{V} \leftarrow \mathbf{V} \circ \frac{\lambda_2 \mathbf{E}^\top \mathbf{H} + \lambda_3 \mathbf{U}}{(\lambda_2 \mathbf{E}^\top \mathbf{E} + D)\mathbf{V}} \quad (2.26)$$

5. **Update the community indicator matrix  $\mathbf{C}$  for pathways.** In a similar process, we fix  $\mathbf{K}$ , and update  $\mathbf{C}$ . The matrix  $\mathbf{C}$  is updated such that the error is minimized:

$$\begin{aligned} \mathcal{J}(\mathbf{C}) = & -\text{tr}(\mathbf{A}^{\text{prox}\top} \mathbf{P} \mathbf{T} \mathbf{C}^\top) - \text{tr}(\mathbf{C} \mathbf{T}^\top \mathbf{P}^\top \mathbf{A}^{\text{prox}}) + \text{tr}(\mathbf{C} \mathbf{T}^\top \mathbf{P}^\top \mathbf{P} \mathbf{T} \mathbf{C}^\top) \\ & + \alpha \left( \text{tr}(\mathbf{C}^\top \mathbf{C} \mathbf{C}^\top \mathbf{C}) - 2\text{tr}(\mathbf{C}^\top \mathbf{C}) \right) + \lambda_5 \text{tr}(\mathbf{C}^\top \mathbf{C}) + \text{tr}(\varpi \mathbf{C}) \\ & - \text{tr}(\mathbf{Y}^\top \mathbf{L} \mathbf{T} \mathbf{C}^\top) - \text{tr}(\mathbf{C} \mathbf{T}^\top \mathbf{L}^\top \mathbf{Y}) + \text{tr}(\mathbf{C} \mathbf{T}^\top \mathbf{L}^\top \mathbf{L} \mathbf{T} \mathbf{C}^\top) \end{aligned} \quad (2.27)$$

Taking the derivative of this error with respect to  $\mathbf{C}$  to 0, we have:

$$\varpi = 2\mathbf{A}^{\text{prox}\top} \mathbf{P} \mathbf{T} + 2\mathbf{Y}^\top \mathbf{L} \mathbf{T} + 4\alpha \mathbf{C} - 2\mathbf{C}(\mathbf{T}^\top \mathbf{P}^\top \mathbf{P} \mathbf{T} + \mathbf{T}^\top \mathbf{L}^\top \mathbf{L} \mathbf{T} + 2\alpha \mathbf{C}^\top \mathbf{C} + \lambda_5) \quad (2.28)$$

Again, we follow the Karush–Kuhn–Tucker conditions for the nonnegativity of  $\mathbf{C}$

$$2\left(\mathbf{A}^{\text{prox}\top} \mathbf{P} \mathbf{T} + \mathbf{Y}^\top \mathbf{L} \mathbf{T} + 2\alpha \mathbf{C} - \mathbf{C}(\mathbf{T}^\top \mathbf{P}^\top \mathbf{P} \mathbf{T} + \mathbf{T}^\top \mathbf{L}^\top \mathbf{L} \mathbf{T} + 2\alpha \mathbf{C}^\top \mathbf{C} + \lambda_5)\right)_{j,k} \mathbf{C}_{j,k} = \varpi_{j,k} \mathbf{C}_{j,k} = 0 \quad (2.29)$$

The parameter  $\mathbf{C}$  is updated according:

$$\mathbf{C} \leftarrow \mathbf{C} \circ \frac{\mathbf{A}^{\text{prox}\top} \mathbf{P} \mathbf{T} + \mathbf{Y}^\top \mathbf{L} \mathbf{T} + 2\alpha \mathbf{C}}{\mathbf{C}(\mathbf{T}^\top \mathbf{P}^\top \mathbf{P} \mathbf{T} + \mathbf{T}^\top \mathbf{L}^\top \mathbf{L} \mathbf{T} + 2\alpha \mathbf{C}^\top \mathbf{C} + \lambda_5)} \quad (2.30)$$

6. **Update the community indicator matrix  $\mathbf{K}$  for ECs.** Once the parameter  $\mathbf{C}$  is updated, we use it to update  $\mathbf{K}$ . The matrix  $\mathbf{K}$  is updated such that the error is minimized:

$$\begin{aligned} \mathcal{J}(\mathbf{K}) = & -\text{tr}(\mathbf{B}^{\text{prox}\top} \mathbf{E} \mathbf{R} \mathbf{K}^\top) - \text{tr}(\mathbf{K} \mathbf{R}^\top \mathbf{E}^\top \mathbf{B}^{\text{prox}}) + \text{tr}(\mathbf{K} \mathbf{R}^\top \mathbf{E}^\top \mathbf{E} \mathbf{R} \mathbf{K}^\top) \\ & + \beta \left( \text{tr}(\mathbf{K}^\top \mathbf{K} \mathbf{K}^\top \mathbf{K}) - 2\text{tr}(\mathbf{K}^\top \mathbf{K}) \right) + \lambda_5 \text{tr}(\mathbf{K}^\top \mathbf{K}) + \text{tr}(\xi \mathbf{K}) \\ & - \text{tr}(\mathbf{X}^\top \mathbf{L} \mathbf{R} \mathbf{K}^\top) - \text{tr}(\mathbf{K} \mathbf{R}^\top \mathbf{L}^\top \mathbf{X}) + \text{tr}(\mathbf{K} \mathbf{R}^\top \mathbf{L}^\top \mathbf{L} \mathbf{R} \mathbf{K}^\top) \end{aligned} \quad (2.31)$$

Taking the derivative of this error with respect to  $\mathbf{K}$  to 0, we have:

$$\xi = 2\mathbf{B}^{\text{prox}\top} \mathbf{E} \mathbf{R} + 2\mathbf{X}^\top \mathbf{L} \mathbf{R} + 4\beta \mathbf{K} - 2\mathbf{K}(\mathbf{R}^\top \mathbf{E}^\top \mathbf{E} \mathbf{R} + \mathbf{R}^\top \mathbf{L}^\top \mathbf{L} \mathbf{R} + 2\beta \mathbf{K}^\top \mathbf{K} + \lambda_5) \quad (2.32)$$

Using the Karush–Kuhn–Tucker conditions for the nonnegativity of  $\mathbf{K}$ , we obtain:

$$2\left(\mathbf{B}^{\text{prox}\top} \mathbf{E} \mathbf{R} + \mathbf{X}^\top \mathbf{L} \mathbf{R} + 2\beta \mathbf{K} - \mathbf{K}(\mathbf{R}^\top \mathbf{E}^\top \mathbf{E} \mathbf{R} + \mathbf{R}^\top \mathbf{L}^\top \mathbf{L} \mathbf{R} + 2\beta \mathbf{K}^\top \mathbf{K} + \lambda_5)\right)_{j,k} \mathbf{K}_{j,k} = \xi_{j,k} \mathbf{K}_{j,k} = 0 \quad (2.33)$$

The parameter  $\mathbf{K}$  is updated according:

$$\mathbf{K} \leftarrow \mathbf{K} \circ \frac{\mathbf{B}^{\text{prox}\top} \mathbf{E} \mathbf{R} + \mathbf{X}^\top \mathbf{L} \mathbf{R} + 2\beta \mathbf{K}}{\mathbf{K}(\mathbf{R}^\top \mathbf{E}^\top \mathbf{E} \mathbf{R} + \mathbf{R}^\top \mathbf{L}^\top \mathbf{L} \mathbf{R} + 2\beta \mathbf{K}^\top \mathbf{K} + \lambda_5)} \quad (2.34)$$

7. **Update the community representation matrix  $\mathbf{T}$  for pathways.** By fixing the parameters  $\mathbf{C}$ ,  $\mathbf{R}$ , and  $\mathbf{K}$ , we update  $\mathbf{T}$ . The matrix  $\mathbf{T}$  is updated such that the error is minimized:

$$\begin{aligned} \mathcal{J}(\mathbf{T}) = & -\text{tr}(\mathbf{A}^{\text{prox}\top} \mathbf{P} \mathbf{T} \mathbf{C}^\top) - \text{tr}(\mathbf{C} \mathbf{T}^\top \mathbf{P}^\top \mathbf{A}^{\text{prox}}) + \text{tr}(\mathbf{C} \mathbf{T}^\top \mathbf{P}^\top \mathbf{P} \mathbf{T} \mathbf{C}^\top) - \text{tr}(\mathbf{Y}^\top \mathbf{L} \mathbf{T} \mathbf{C}^\top) \\ & - \text{tr}(\mathbf{C} \mathbf{T}^\top \mathbf{L}^\top \mathbf{Y}) + \text{tr}(\mathbf{C} \mathbf{T}^\top \mathbf{L}^\top \mathbf{L} \mathbf{T} \mathbf{C}^\top) + \lambda_5 \text{tr}(\mathbf{T}^\top \mathbf{T}) + \text{tr}(\zeta \mathbf{T}) \end{aligned} \quad (2.35)$$

Taking the derivative of this error with respect to  $\mathbf{T}$  to 0, we have:

$$\zeta = 2\mathbf{P}^\top \mathbf{A}^{\text{prox}} \mathbf{C} + 2\mathbf{L}^\top \mathbf{Y} \mathbf{C} - 2(\mathbf{P}^\top \mathbf{C} \mathbf{C}^\top \mathbf{P} + \lambda_5) \mathbf{T} - 2\mathbf{L}^\top \mathbf{L} \mathbf{T} \mathbf{C}^\top \mathbf{C} \quad (2.36)$$

Using the Karush–Kuhn–Tucker conditions for the nonnegativity of  $\mathbf{T}$ , we obtain:

$$2\left(\mathbf{P}^\top \mathbf{A}^{\text{prox}} \mathbf{C} + \mathbf{L}^\top \mathbf{Y} \mathbf{C} - (\mathbf{P}^\top \mathbf{C} \mathbf{C}^\top \mathbf{P} + \lambda_5) \mathbf{T} - \mathbf{L}^\top \mathbf{L} \mathbf{T} \mathbf{C}^\top \mathbf{C}\right)_{j,k} \mathbf{T}_{j,k} = \zeta_{j,k} \mathbf{T}_{j,k} = 0 \quad (2.37)$$

The parameter  $\mathbf{T}$  is updated according:

$$\mathbf{T} \leftarrow \mathbf{T} \circ \frac{\mathbf{P}^\top \mathbf{A}^{\text{prox}} \mathbf{C} + \mathbf{L}^\top \mathbf{Y} \mathbf{C}}{(\mathbf{P}^\top \mathbf{C} \mathbf{C}^\top \mathbf{P} + \lambda_5) \mathbf{T} + \mathbf{L}^\top \mathbf{L} \mathbf{T} \mathbf{C}^\top \mathbf{C}} \quad (2.38)$$

8. **Update the community representation matrix  $\mathbf{R}$  for EC features.** By fixing the parameters  $\mathbf{C}$ ,  $\mathbf{T}$ , and  $\mathbf{K}$ , we update  $\mathbf{R}$ . The matrix  $\mathbf{R}$  is updated such that the error is minimized:

$$\begin{aligned} \mathcal{J}(\mathbf{R}) = & -\text{tr}(\mathbf{B}^{\text{prox}\top} \mathbf{E} \mathbf{R} \mathbf{K}^\top) - \text{tr}(\mathbf{K} \mathbf{R}^\top \mathbf{E}^\top \mathbf{B}^{\text{prox}}) + \text{tr}(\mathbf{K} \mathbf{R}^\top \mathbf{E}^\top \mathbf{E} \mathbf{R} \mathbf{K}^\top) - \text{tr}(\mathbf{X}^\top \mathbf{L} \mathbf{R} \mathbf{K}^\top) \\ & - \text{tr}(\mathbf{K} \mathbf{R}^\top \mathbf{L}^\top \mathbf{X}) + \text{tr}(\mathbf{K} \mathbf{R}^\top \mathbf{L}^\top \mathbf{L} \mathbf{R} \mathbf{K}^\top) + \lambda_5 \text{tr}(\mathbf{R}^\top \mathbf{R}) + \text{tr}(\kappa \mathbf{R}) \end{aligned} \quad (2.39)$$

Taking the derivative of this error with respect to  $\mathbf{R}$  to 0, we have:

$$\kappa = 2\mathbf{E}^\top \mathbf{B}^{\text{prox}} \mathbf{K} + 2\mathbf{L}^\top \mathbf{X} \mathbf{K} - 2(\mathbf{E}^\top \mathbf{K} \mathbf{K}^\top \mathbf{E} + \lambda_5) \mathbf{R} - 2\mathbf{L}^\top \mathbf{L} \mathbf{R} \mathbf{K}^\top \mathbf{K} \quad (2.40)$$

Using the Karush–Kuhn–Tucker conditions for the nonnegativity of  $\mathbf{R}$ , we obtain:

$$2\left(\mathbf{E}^\top \mathbf{B}^{\text{prox}} \mathbf{K} + \mathbf{L}^\top \mathbf{X} \mathbf{K} - (\mathbf{E}^\top \mathbf{K} \mathbf{K}^\top \mathbf{E} + \lambda_5) \mathbf{R} - \mathbf{L}^\top \mathbf{L} \mathbf{R} \mathbf{K}^\top \mathbf{K}\right)_{j,k} \mathbf{R}_{j,k} = \kappa_{j,k} \mathbf{R}_{j,k} = 0 \quad (2.41)$$

The parameter  $\mathbf{R}$  is updated according:

$$\mathbf{R} \leftarrow \mathbf{R} \circ \frac{\mathbf{E}^\top \mathbf{B}^{\text{prox}} \mathbf{K} + \mathbf{L}^\top \mathbf{X} \mathbf{K}}{(\mathbf{E}^\top \mathbf{K} \mathbf{K}^\top \mathbf{E} + \lambda_5) \mathbf{R} + \mathbf{L}^\top \mathbf{L} \mathbf{R} \mathbf{K}^\top \mathbf{K}} \quad (2.42)$$

9. **Update the weight matrix  $\Theta$ .** By fixing the other parameters, we update  $\Theta$ . The matrix  $\Theta$  is updated such that the error is minimized:

$$\begin{aligned} \mathcal{J}^{\text{path}}(\Theta) = & \sum_{i \in n} \sum_{k \in t} \log\left(1 + e^{-\mathbf{y}_k^{(i)} \Theta_k^\top \mathbf{x}^{(i)}}\right) + \rho\left(\text{tr}(\Theta^\top \Theta) - \text{tr}(\Theta^\top \mathbf{Z} \mathbf{H} \mathbf{W}^\top)\right. \\ & \left. - \text{tr}(\mathbf{W} \mathbf{H}^\top \mathbf{Z}^\top \Theta)\right) + \lambda_6 \|\Theta\|_{2,1} \end{aligned} \quad (2.43)$$

where  $f(\cdot)$  is a non-linear sigmoid function, i.e.,  $f(x) = \sigma(x) = \frac{1}{1+e^{-x}}$ . This choice can be generalized to any non-linear functions. By transforming  $\mathbf{X}$  with  $\sigma(\cdot)$  and  $\Theta$ , our method enables pathway prediction. Taking the derivative of this error with respect to  $\Theta$  to 0, we have:

$$\nabla_{\Theta} \mathcal{J}^{\text{path}}(\Theta) = \frac{1}{n} \sum_{i \in n} \sum_{k \in t} \left( \frac{-\mathbf{y}_k^{(i)} \mathbf{x}^{(i)}}{1 + e^{\mathbf{y}_k^{(i)} \Theta_k^\top \mathbf{x}^{(i)}}} \right) + 2\rho(\Theta - \mathbf{Z} \mathbf{H} \mathbf{W}^\top) + \lambda_6 \text{tr}\left(\frac{\Theta}{2\|\Theta\|_{2,1}}\right) \quad (2.44)$$

Due to non-closed form of the above equation, we use iterative gradient descent approach with a defined learning rate  $\eta$ . Hence, the general update rule for  $\Theta$  becomes:

$$\Theta^{i+1} \leftarrow \Theta^i - \eta \circ \nabla_{\Theta} \mathcal{J}^{\text{path}}(\Theta^i) \quad (2.45)$$

10. **Update the auxiliary matrix  $\mathbf{L}$ .** By fixing the rest of parameters in  $\mathcal{J}^{\text{path}}$ , the matrix  $\mathbf{L}$  is updated such that the error is minimized:

$$\begin{aligned} \mathcal{J}^{\text{path}}(\mathbf{L}) = & -\text{tr}(\mathbf{X}^{\top} \mathbf{L} \mathbf{R} \mathbf{K}^{\top}) - \text{tr}(\mathbf{K} \mathbf{R}^{\top} \mathbf{L}^{\top} \mathbf{X}) + \text{tr}(\mathbf{K} \mathbf{R}^{\top} \mathbf{L}^{\top} \mathbf{L} \mathbf{R} \mathbf{K}^{\top}) - \text{tr}(\mathbf{Y}^{\top} \mathbf{L} \mathbf{T} \mathbf{C}^{\top}) \\ & - \text{tr}(\mathbf{C} \mathbf{T}^{\top} \mathbf{L}^{\top} \mathbf{Y}) + \text{tr}(\mathbf{C} \mathbf{T}^{\top} \mathbf{L}^{\top} \mathbf{L} \mathbf{T} \mathbf{C}^{\top}) + \lambda_6 \text{tr}(\mathbf{L}^{\top} \mathbf{L}) \end{aligned} \quad (2.46)$$

Taking the derivative of this error with respect to  $\mathbf{L}$  to 0, we have:

$$\nabla_{\mathbf{L}} \mathcal{J}^{\text{path}}(\mathbf{L}) = 2(\mathbf{L} \mathbf{T} \mathbf{C}^{\top} \mathbf{C} \mathbf{T}^{\top} + \mathbf{L} \mathbf{R} \mathbf{K}^{\top} \mathbf{K} \mathbf{R}^{\top} - \mathbf{Y} \mathbf{C} \mathbf{T}^{\top} - \mathbf{X} \mathbf{K} \mathbf{R}^{\top} + \lambda_6 \mathbf{L}) \quad (2.47)$$

The parameter  $\mathbf{L}$  is updated according:

$$\mathbf{L}^{i+1} \leftarrow \mathbf{L}^i - \eta \circ \nabla_{\mathbf{L}} \mathcal{J}^{\text{path}}(\mathbf{L}^i) \quad (2.48)$$

11. **Update the auxiliary matrix  $\mathbf{Z}$ .** By fixing the rest of parameters in  $\mathcal{J}^{\text{path}}$ , the matrix  $\mathbf{Z}$  is updated such that the error is minimized:

$$\mathcal{J}^{\text{path}}(\mathbf{Z}) = -\rho \text{tr}(\Theta^{\top} \mathbf{Z} \mathbf{H} \mathbf{W}^{\top}) - \rho \text{tr}(\mathbf{W} \mathbf{H}^{\top} \mathbf{Z}^{\top} \Theta) + \rho \text{tr}(\mathbf{W} \mathbf{H}^{\top} \mathbf{Z}^{\top} \mathbf{Z} \mathbf{H} \mathbf{W}^{\top}) + \lambda_6 \text{tr}(\mathbf{Z}^{\top} \mathbf{Z}) \quad (2.49)$$

Taking the derivative of this error with respect to  $\mathbf{Z}$  to 0, we have:

$$\nabla_{\mathbf{Z}} \mathcal{J}^{\text{path}}(\mathbf{Z}) = 2(\rho \mathbf{Z} \mathbf{H} \mathbf{W}^{\top} \mathbf{W} \mathbf{H}^{\top} - \rho \Theta \mathbf{W} \mathbf{H}^{\top} + \lambda_6 \mathbf{Z}) \quad (2.50)$$

The parameter  $\mathbf{Z}$  is updated according to gradient descent approach as:

$$\mathbf{Z}^{i+1} \leftarrow \mathbf{Z}^i - \eta \circ \nabla_{\mathbf{Z}} \mathcal{J}^{\text{path}}(\mathbf{Z}^i) \quad (2.51)$$

### 3 Dataset Characteristics

We report the performance of triUMPF using i)- T1 golden dataset consisting of six PGDBs from the BioCyc collection (biocyc) including *EcoCyc* (v21), *HumanCyc* (v19.5), *AraCyc* (v18.5), *YeastCyc* (v19.5), *LeishCyc* (v19.5), and *TrypanoCyc* (v18.5), ii)- low complexity data from *Moranella* (GenBank NC-015735) and *Tremblaya* (GenBank NC-015736) symbiont genomes encoding distributed metabolic pathways for amino acid biosynthesis ([10]), iii)- the Critical Assessment of Metagenome Interpretation (CAMI) initiative low complexity dataset (edwards.sdsu.edu/research/cami-challenge-datasets/), consisting of 40 genomes ([12]), and iv)- whole genome shotgun sequences from the Hawaii Ocean Time Series (HOTS) at 25m, 75m, 110m (sunlit) and 500m (dark) ocean depth intervals downloaded from the NCBI Sequence Read Archive under accession numbers SRX007372, SRX007369, SRX007370, SRX007371 ([13]). T1 PGDBs were refined to include only those pathways that cross-intersect with the *MetaCyc* database (v21) ([1]). Training data was obtained from BioCyc (v20.5 T2 & 3) ([2]), consisting of 9255 Pathway/Genome Databases (PGDBs) with 1463 distinct pathway labels constructed using the Pathway Tools software ([6]). The detailed characteristics of the datasets are summarized in Table 1. For each dataset  $\mathcal{S}$ , we use  $|\mathcal{S}|$  and  $L(\mathcal{S})$  to represent the number of instances and pathway labels, respectively. In addition, we also present some characteristics of the multi-label datasets, which are denoted as:

1. Label cardinality ( $L\text{Card}(\mathcal{S}) = \frac{1}{n} \sum_{i=1}^n \sum_{j=1}^t \mathbb{I}[\mathbf{Y}_{i,j} \neq -1]$ ), where  $\mathbb{I}$  is an indicator function. It denotes the average number of pathways in  $\mathcal{S}$ .
2. Label density ( $L\text{Den}(\mathcal{S}) = \frac{L\text{Card}(\mathcal{S})}{L(\mathcal{S})}$ ). This is simply obtained through normalizing  $L\text{Card}(\mathcal{S})$  by the number of total pathways in  $\mathcal{S}$ .
3. Distinct label sets ( $DL(\mathcal{S})$ ). This notation indicates the number of distinct pathways in  $\mathcal{S}$ .
4. Proportion of distinct label sets ( $PDL(\mathcal{S}) = \frac{DL(\mathcal{S})}{|\mathcal{S}|}$ ). It represents the normalized version of  $DL(\mathcal{S})$ , and is obtained by dividing  $DL(\cdot)$  with the number of instances in  $\mathcal{S}$ .

The notations  $R(\mathcal{S})$ ,  $R\text{Card}(\mathcal{S})$ ,  $R\text{Den}(\mathcal{S})$ ,  $DR(\mathcal{S})$ , and  $PDR(\mathcal{S})$  have similar meanings for the enzymatic reactions  $\mathcal{E}$  in  $\mathcal{S}$ . Finally,  $\text{PLR}(\mathcal{S})$  represents a ratio of  $L(\mathcal{S})$  to  $R(\mathcal{S})$ .

Dataset	$ \mathcal{S} $	$L(\mathcal{S})$	$L\text{Card}(\mathcal{S})$	$L\text{Den}(\mathcal{S})$	$DL(\mathcal{S})$	$PDL(\mathcal{S})$	$R(\mathcal{S})$	$R\text{Card}(\mathcal{S})$	$R\text{Den}(\mathcal{S})$	$DR(\mathcal{S})$	$PDR(\mathcal{S})$	$PLR(\mathcal{S})$	Domain
AraCyc	1	510	510	1	510	510	2182	2182	1	1034	1034	0.2337	Arabidopsis thaliana
EcoCyc	1	307	307	1	307	307	1134	1134	1	719	719	0.2707	Escherichia coli K-12 substr.MG1655
HumanCyc	1	279	279	1	279	279	1177	1177	1	693	693	0.2370	Homo sapiens
LeishCyc	1	87	87	1	87	87	363	363	1	292	292	0.2397	Leishmania major Friedlin
TrypanoCyc	1	175	175	1	175	175	743	743	1	512	512	0.2355	Trypanosoma brucei
YeastCyc	1	229	229	1	229	229	966	966	1	544	544	0.2371	Saccharomyces cerevisiae
Symbiotic	3	119	39.6667	0.3333	59	19.6667	304	101.3333	0.3333	130	43.3333	0.3914	Composed of Moranella and Tremblaya
CAMI	40	6261	156.5250	0.0250	674	16.8500	14269	356.7250	0.0250	1083	27.0750	0.4388	Simulated microbiomes of low complexity
HOT	4	2178	311.1429	0.1429	781	111.5714	182675	26096.4286	0.1429	1442	206.0000	0.0119	Metagenomic Hawaii Ocean Time-series (10m, 75m, 110m, and 500m)
BioCyc	9255	1804003	194.9220	0.0001	1463	0.1581	8848714	956.1009	0.0001	2705	0.2923	0.2039	BioCyc version 20.5 (tier 2 & 3)

Table 1: Characteristics of the experimental datasets. The notations  $|\mathcal{S}|$ ,  $L(\mathcal{S})$ ,  $L\text{Card}(\mathcal{S})$ ,  $L\text{Den}(\mathcal{S})$ ,  $DL(\mathcal{S})$ , and  $PDL(\mathcal{S})$  represent: number of instances, number of pathway labels, pathway labels cardinality, pathway labels density, distinct pathway labels set, and proportion of distinct pathway labels set for  $\mathcal{S}$ , respectively. The notations  $R(\mathcal{S})$ ,  $R\text{Card}(\mathcal{S})$ ,  $R\text{Den}(\mathcal{S})$ ,  $DR(\mathcal{S})$ , and  $PDR(\mathcal{S})$  have similar meanings for the enzymatic reactions  $\mathcal{E}$  in  $\mathcal{S}$ .  $PLR(\mathcal{S})$  represents a ratio of  $L(\mathcal{S})$  to  $R(\mathcal{S})$ . The last column denotes the domain of  $\mathcal{S}$ .

## 4 Incorporating EC Features

For pathway prediction, the EC features are concatenated into each example  $i$  according to:

$$\tilde{\mathbf{x}}^{(i)} = \mathbf{x}^{(i)} \oplus \frac{1}{r} \mathbf{x}^{(i)} \mathbf{E} \quad (4.1)$$

where  $\oplus$  indicates the vector concatenation operation,  $\mathbf{E} \in \mathbb{R}^{r \times m}$  corresponds the feature matrix of ECs and  $m = 128$ . The addition of features results in a dimension of size  $r + m$ , where  $r = 3650$ . We expect by incorporating enzymatic reactions features into the original  $r$  dimensional example  $\mathbf{x}^{(i)}$ , the modified  $\tilde{\mathbf{x}}^{(i)}$  summarizes informative characteristics, which are likely to be useful in the prediction task.

### 4.1 Parameter Sensitivity

Fig. 1 shows the effect of rank  $k$  on triUMPF performance. In general, we observe that the performance is static across  $k$  values. This is in contrast to standard NMF where the reconstruction cost decreases as the number of features increases. This is expected because, unlike standard NMF, triUMPF exploits two types of correlations to recover  $\mathbf{M}$ : i)- within ECs or pathways and ii)- betweenness interactions, hence, serving as additional regularizers. As observed from Fig. 1, higher  $k$  ( $k = 100$ ) values result in improved outcomes.

## 5 Network Reconstruction

In this section, we examined the robustness of triUMPF when exposed to noise. As indicated in the main manuscript, links were randomly removed from  $\mathbf{M}$ ,  $\mathbf{A}$ , and  $\mathbf{B}$  according to  $\epsilon \in \{20\%, 40\%, 60\%, 80\%\}$ . We used the partially linked matrices to refine parameters while comparing the reconstruction cost against the full association matrices  $\mathbf{M}$ ,  $\mathbf{A}$  and  $\mathbf{B}$ . Specifically for  $\mathbf{M}$ , we varied components of  $\mathbf{M}$  according to  $k \in \{20, 50, 70, 90, 120\}$  along with  $\epsilon$ . For all experiments, BioCyc was used for training using the hyperparameters described in the paper Section 3.4.

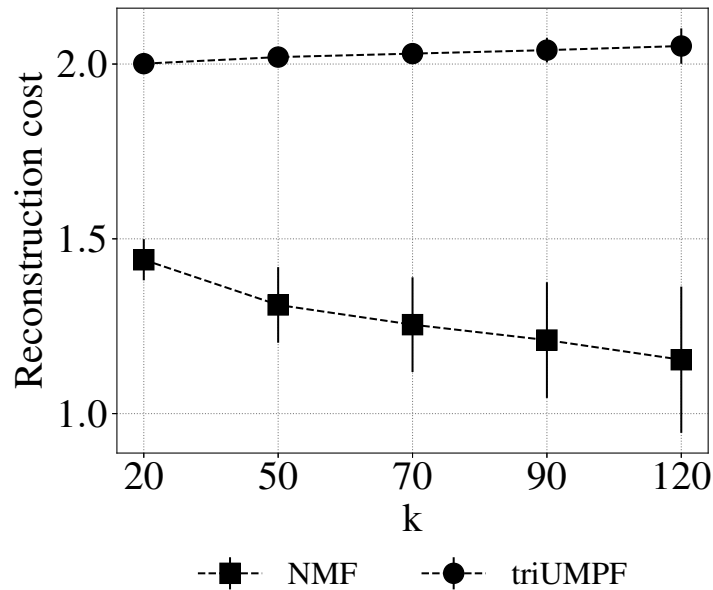


Figure 1: Sensitivity of components  $k$  based on reconstruction cost.

Fig. 3a shows that, in general, by progressively increasing noise  $\varepsilon$  to  $\mathbf{M}$ , the reconstruction cost increases when  $k$  is low. As more features are incorporated the cost at all noise levels steadily decreases up to  $k = 100$ . This tendency indicates that both pathway and EC features ( $\mathbf{P}$  and  $\mathbf{E}$  contain useful correlations that contribute to the resilience of triUMPF’s performance when  $\mathbf{M}$  is perturbed. For  $\mathbf{A}^{\text{prox}}$  and  $\mathbf{B}^{\text{prox}}$ , as shown in Supp Figs 3b and 3b, the costs are reduced in the presence of noise, which is not surprising as the reconstruction of associated communities are constrained on both data and  $\mathbf{A}^{\text{prox}}$  and  $\mathbf{B}^{\text{prox}}$ . These results are directly linked to the sparseness of both matrices, as previously described in ([4]). For community detection, it is sufficient to group nodes that are densely connected, while links between communities can remain sparse. The same line of reasoning follows for the EC network.

## 6 Visualization

We compared the Pathologic predicted pathways with triUMPF’s results on MG1655 where its true pathways can be obtained from golden T1 EcoCyc. Fig. 4 shows pathways predicted from MG1655 4a, CFT073 4b, and EDL933 4c by both Pathologic (taxonomic pruning) and triUMPF methods. Since true pathways of MG1655 can be obtained from golden T1 EcoCyc, we have extra color coding for nodes.

Table 2 outlines the top 5 community indices with their associated pathways as predicted by triUMPF for the Escherichia coli K-12 substr. MG1655 (TAX-511145). Since the pathway information of this species is encoded in EcoCyc, it is possible to determine the true pathways (indicated by the “Status” column in the table) by mapping the predicted pathways onto EcoCyc. As can be seen, pathways in Table 2 were inferred as a consequence of communities.

Fig. 5 shows 18 amino acid pathways predicted by triUMPF and PathoLogic (taxonomic pruning) according to GapMind [11] for the three strains where each reconstructed pathway is supported by a confidence level. We excluded pathways that were not incorporated in the training set. This resulted in a total of 102 pathways identified across the three strains encompassing 18 amino acid biosynthetic pathways and 27 pathway variants with high confidence (Table 3). In contrast, PathoLogic inferred 49 pathways identified across the three strains encompassing 16 amino acid biosynthetic pathways and 17 pathway variants while triUMPF inferred 51 pathways identified across the three strains encompassing 17 amino acid biosynthetic pathways and 19 pathway variants including *L-methionine biosynthesis* in K-12, CFT073 and EDL933 that was not predicted by PathoLogic. Neither method was able to predict *L-tyrosine biosynthesis I*.

We also analyzed pathways using non taxonomic pruning option for PathoLogic. Fig. 6 shows that PathoLogic infers more pathways that may not correspond to prokaryotes. To validate this observation, we invoked GapMind [11] to analyze 18 amino acid biosynthesis pathways. Based on GapMind results, PathoLogic inferred 56 pathways identified across the three strains encompassing 15 amino acid biosynthetic pathways and 21 pathway variants, including *L-proline biosynthesis II (from arginine)* pathway that is known only for eukaryotes.

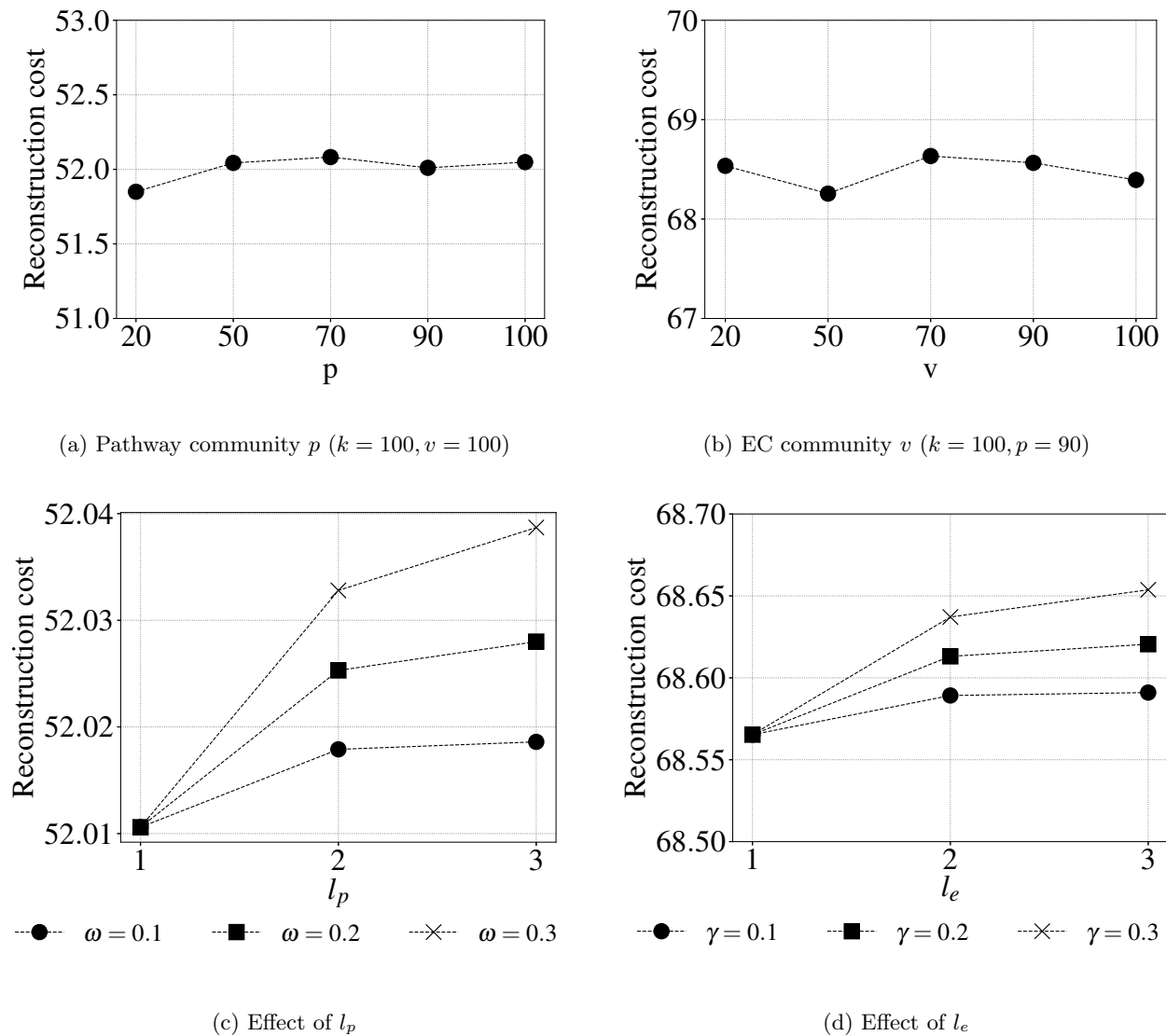


Figure 2: Sensitivity of community size and higher order proximity with weights based on reconstruction cost.

## 7 Metabolic Pathway Prediction

Here, we investigate the effectiveness of triUMPF for the pathway prediction task on T1 golden datasets, Symbiont [10], CAMI low complexity data [12], and HOTS datasets [13].

### 7.1 Impact of $\rho$

Fig. 8 shows the inverse effect in predictive performance on T1 golden datasets when decreasing the  $\rho$  before reaching a performance plateau at  $\rho = 0.001$ . This suggests, in practice, lesser constraints should be emphasized on  $\Theta$ , while not neglecting associations between EC numbers and pathways indicated in  $\mathbf{M}$ .

### 7.2 Pathway Prediction from Golden data

For this case study, we compare the performance of triUMPF on 6 benchmark datasets, as described in Section 3, against the other pathway prediction algorithms using four evaluation metrics: *Hamming loss*, *average precision*, *average recall*, and *average F1 score*. As shown in Table 4, triUMPF achieved competitive performance against the other methods in terms of average precision. In particular, triUMPF yielded 0.8662 (average precision) on EcoCyc. However, w.r.t. average F1 scores, it underperformed on HumanCyc and AraCyc, yielding average F1 scores of 0.4703 and 0.4775, respectively. This is due to the limited number of pathway labels available for training.

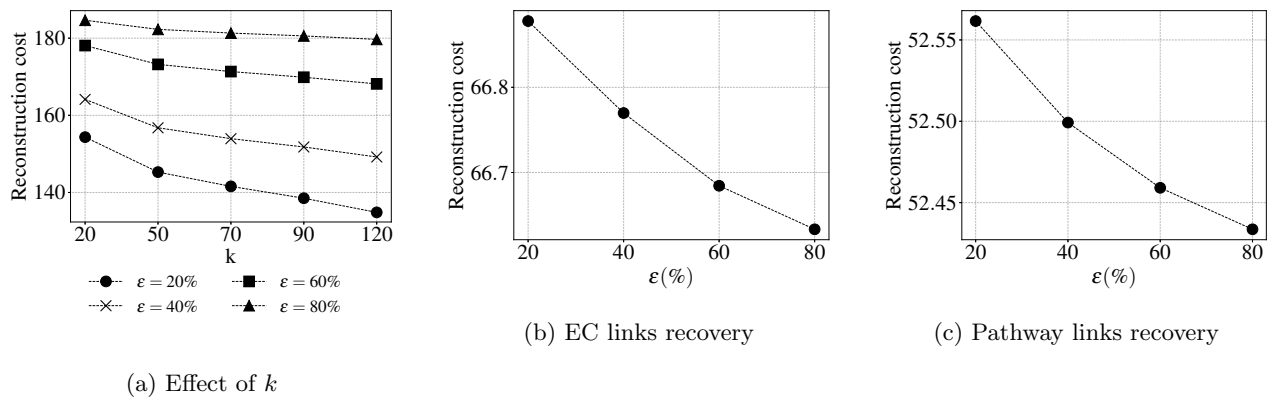


Figure 3: Link prediction results by varying noise levels  $\epsilon \in \{20\%, 40\%, 60\%, 80\%\}$  based on reconstruction cost.

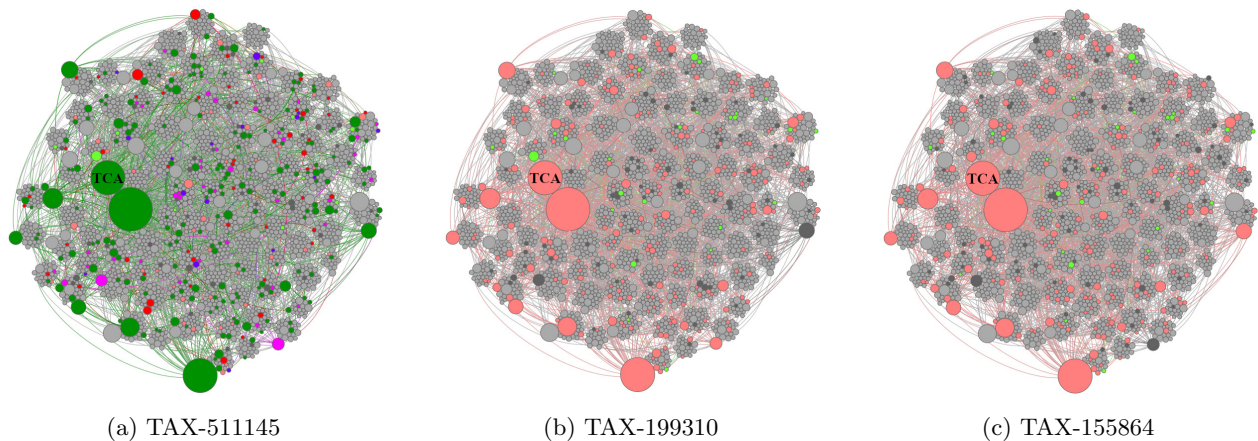


Figure 4: Pathway community networks for related T1 and T3 organismal genomes. Pathway communities for (a) *E. coli* K-12 substr. MG1655 (TAX-511145), (b) *E. coli* str. CFT073 (TAX-199310), and (c) *E. coli* O157:H7 str. EDL933 (TAX-155864) based on community detection. Nodes colored in *dark grey* indicate pathways predicted by PathoLogic; *lime* pathways predicted by triUMPF; *salmon* pathways predicted by both PathoLogic and triUMPF; *red* expected pathways not predicted by both PathoLogic and triUMPF; *magenta* expected pathways predicted only by PathoLogic; *purple* expected pathways predicted solely by triUMPF; and *green* expected pathways predicted by both PathoLogic and triUMPF. *light-grey* indicates pathways not expected to be encoded in either organismal genome. The node sizes reflect the degree of associations between pathways.

### 7.3 Predicted Pathways from Symbiont data

We analyze pathways from each individual genome and their combinations. Fig. 9 shows that both triUMPF and PathoLogic predicted 6 pathways on combined genomes, which again attests the novelty of triUMPF method. For the phenylalanine pathway (*L-phenylalanine biosynthesis I*), genes were reported to be missing during the ORF prediction process, henceforth, we excluded this pathway from outputs. However, both methods inferred some false-positive pathways. For example, Both methods predicted *L-tryptophan biosynthesis* pathway in both *Moranella* and combined, despite it was reported that this pathway requires a set of genes from both *Tremblaya* and *Moranella* ([10]), hence, this pathway should not be recovered for *Moranella*.

### 7.4 Pathway Prediction from CAMI data

In this section, we contrast triUMPF with mLGPR (using elastic net penalty with reaction and pathway evidence features) on CAMI low complexity dataset. From Table 5, we observe that triUMPF outperformed mLGPR, achieving an average F1 score of 0.5864 in compare to 0.4866 for mLGPR. This is outstanding, given the fact triUMPF was trained on a reduced number of labels.

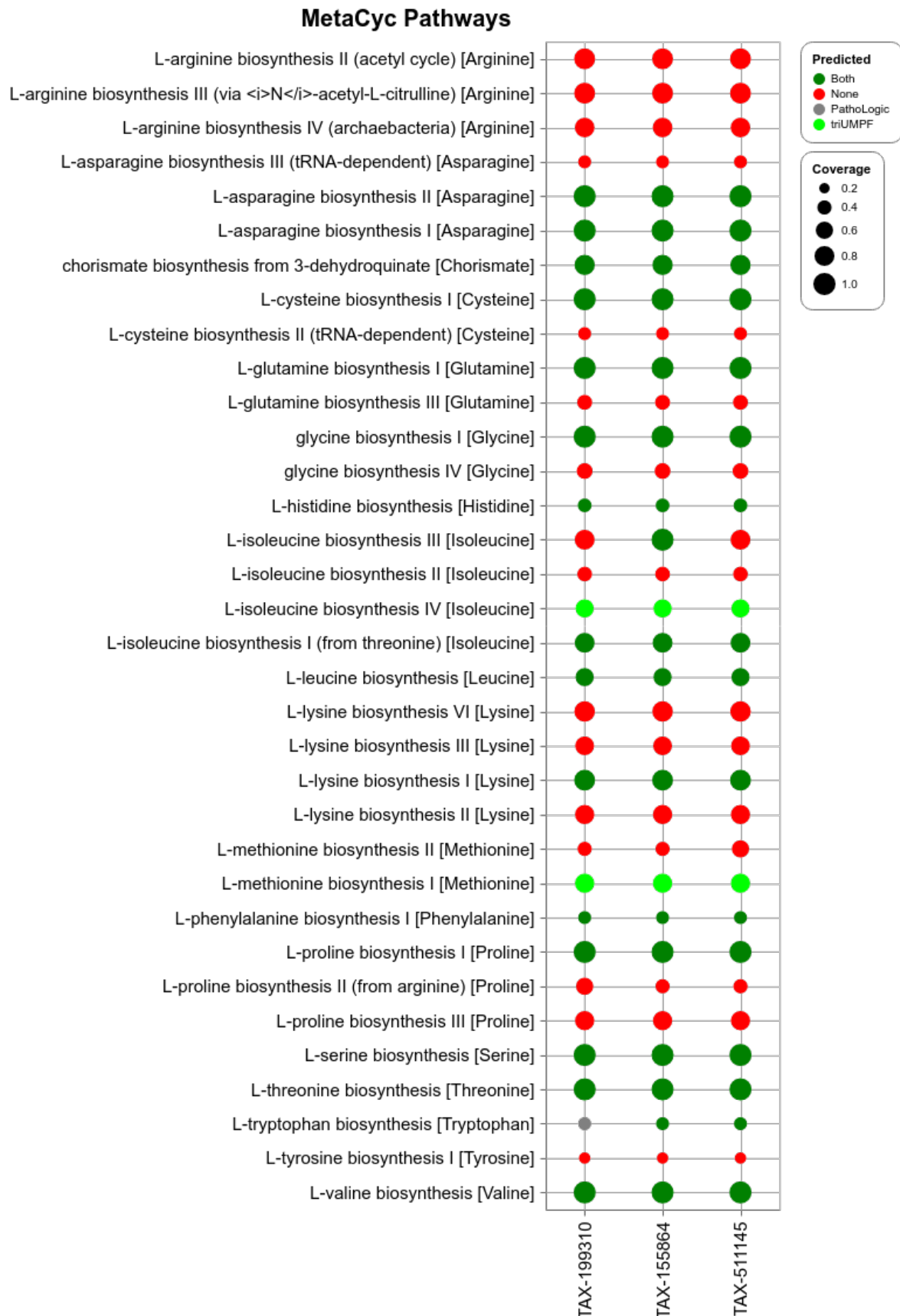


Figure 5: Comparison of predicted pathways for *E. coli* K-12 substr. MG1655 (TAX-511145), *E. coli* str. CFT073 (TAX-199310), and *E. coli* O157:H7 str. EDL933 (TAX-155864) datasets between PathoLogic (taxonomic pruning) and triUMPF. Red circles indicate that neither method predicted a specific pathway while green circles indicate that both methods predicted a specific pathway. Lime circles indicate pathways predicted solely by mLGPR and gray circles indicate pathways solely predicted by PathoLogic. The size of circles corresponds to the associated coverage information.



Community Index	MetaCyc Pathway ID	MetaCyc Pathway Name	Status
67	PWY0-1182	trehalose degradation II (trehalase)	true
	PWY-6910	hydroxymethylpyrimidine salvage	true
	HOMOSER-THRESYN-PWY	L-threonine biosynthesis	true
	PUTDEG-PWY	putrescine degradation I	true
	PWY-6611	adenine and adenosine salvage V	true
	FERMENTATION-PWY	mixed acid fermentation	true
	ENTNER-DOUDOROFF-PWY	Entner-Doudoroff pathway I	true
34	ASPARAGINESYN-PWY	L-asparagine biosynthesis II	true
	PWY-5340	sulfate activation for sulfonation	true
	PWY-6618	guanine and guanosine salvage III	true
	PWY0-1314	fructose degradation	true
	PWY-7181	pyrimidine deoxyribonucleosides degradation	true
	PWY0-1299	arginine dependent acid resistance	true
	PWY0-42	2-methylcitrate cycle I	true
9	NAGLIPASYN-PWY	lipid-A-precursor biosynthesis (E. coli)	true
	PWY-7221	guanosine ribonucleotides de novo biosynthesis	true
	KDOSYN-PWY	Kdo transfer to lipid IV <sub>A</sub> I (E. coli)	true
	PWY0-1309	chitobiose degradation	true
	PPGPPMET-PWY	ppGpp biosynthesis	true
	PWY-6608	guanosine nucleotides degradation III	true
	PWY-5656	mannosylglycerate biosynthesis I	false
47	PLPSAL-PWY	pyridoxal 5'-phosphate salvage I	true
	PWY0-1313	acetate conversion to acetyl-CoA	true
	PYRUVDEHYD-PWY	pyruvate decarboxylation to acetyl CoA	true
	PWY-4381	fatty acid biosynthesis initiation (bacteria and plants)	true
	PWY0-662	PRPP biosynthesis	true
81	HISTSYN-PWY	L-histidine biosynthesis	true
	PWY-6147	6-hydroxymethyl-dihydropterin diphosphate biosynthesis I	true
	PWY-7176	UTP and CTP de novo biosynthesis	true
	PWY-6932	selenate reduction	false

Table 2: Top 5 communities with pathways predicted by triUMPF for *Escherichia coli* K-12 substr. MG1655 (TAX-511145). The last column asserts whether a pathway is present in or absent (a false-positive pathway) from EcoCyc.

## 7.5 Predicted Pathways from HOTS data

We applied triUMPF to infer a set of pathways from HOTS metagenomics data. The results are presented in Fig. 10. Among selected 80 pathways, PathoLogic and triUMPF retrieved a total of 54 and 58 pathways, respectively, while mLGPDR detected 62 pathways. Again this results demonstrate the novelty of triUMPF which is trained on a reduced number of pathways. However, all energy pathways, namely *photosynthesis light reaction* and *pyruvate fermentation to (S)-acetoin*, are not recovered although they are abundant along the water columns. Perhaps, the absence of some ECs associated with those pathways is the prime reason for not detecting them. Indeed it is the case, for example, the enzyme *catabolic acetolactate synthase* (EC-2.2.1.6) is reported to be missing for *pyruvate fermentation to (S)-acetoin* pathway.

## References

- [1] Ron Caspi, Richard Billington, Luciana Ferrer, Hartmut Foerster, Carol A. Fulcher, Ingrid M. Keseler, Anamika Kothari, Markus Krummenacker, Mario Latendresse, Lukas A. Mueller, Quang Ong, Suzanne Paley, Pallavi Subhraveti, Daniel S. Weaver, and Peter D. Karp. The metacyc database of metabolic pathways and enzymes and the biocyc collection of pathway/genome databases. *Nucleic Acids Research*, 44(D1):D471–D480, 2016.
- [2] Ron Caspi, Richard Billington, Hartmut Foerster, Carol A Fulcher, Ingrid Keseler, Anamika Kothari, Markus Krummenacker, Mario Latendresse, Lukas A Mueller, Quang Ong, et al. Biocyc: Online resource for genome and metabolic pathway analysis. *The FASEB Journal*, 30(1 Supplement):1b192–1b192, 2016.
- [3] Andrzej Cichocki, Rafal Zdunek, and Shun-ichi Amari. Hierarchical als algorithms for nonnegative matrix and 3d tensor factorization. In *International Conference on Independent Component Analysis and Signal Separation*, pp. 169–176. Springer, 2007.
- [4] Santo Fortunato and Darko Hric. Community detection in networks: A user guide. *Physics reports*, 659:1–44, 2016.

Amino Acid	MetaCyc Pathway ID	MetaCyc Pathway Name
Arginine	ARGSYNBSUB-PWY	L-arginine biosynthesis II (acetyl cycle)
	PWY-5154	L-arginine biosynthesis III (via N-acetyl-L-citrulline)
	PWY-7400	L-arginine biosynthesis IV (archaeobacteria)
Asparagine	ASPARAGINE-BIOSYNTHESIS	L-asparagine biosynthesis I
	ASPARAGINESYN-PWY	L-asparagine biosynthesis II
Chorismate	PWY-6163	chorismate biosynthesis from 3-dehydroquinate
Cysteine	CYSTSYN-PWY	L-cysteine biosynthesis I
	PWY-6308	L-cysteine biosynthesis II (tRNA-dependent)
Glutamine	GLNSYN-PWY	L-glutamine biosynthesis I
Glycine	GLYSYN-PWY	glycine biosynthesis I
	GLYSYN-THR-PWY	glycine biosynthesis IV
Histidine	HISTSYN-PWY	L-histidine biosynthesis
Isoleucine	ILEUSYN-PWY	L-isoleucine biosynthesis I (from threonine)
	PWY-5104	L-isoleucine biosynthesis IV
Leucine	LEUSYN-PWY	L-leucine biosynthesis
Lysine	DAPLYSINESYN-PWY	L-lysine biosynthesis I
	PWY-2941	L-lysine biosynthesis II
	PWY-2942	L-lysine biosynthesis III
Methionine	HOMOSER-METSYN-PWY	L-methionine biosynthesis I
	PWY-702	L-methionine biosynthesis II
Phenylalanine	PHE SYN	L-phenylalanine biosynthesis I
Proline	PROSYN-PWY	L-proline biosynthesis I
Serine	SERSYN-PWY	L-serine biosynthesis
Threonine	HOMOSER-THRESYN-PWY	L-threonine biosynthesis
Tryptophan	TRPSYN-PWY	L-tryptophan biosynthesis
Tyrosine	TYRSYN	L-tyrosine biosynthesis I
Valine	VALSYN-PWY	L-valine biosynthesis

Table 3: 18 amino acid biosynthetic pathways and 27 pathway variants with high confidence.

- [5] Nicolas Gillis. The why and how of nonnegative matrix factorization. *Regularization, Optimization, Kernels, and Support Vector Machines*, 12(257), 2014.
- [6] Peter D Karp, Mario Latendresse, Suzanne M Paley, Markus Krummenacker, Quang D Ong, Richard Billington, Anamika Kothari, Daniel Weaver, Thomas Lee, Pallavi Subhraveti, et al. Pathway tools version 19.0 update: software for pathway/genome informatics and systems biology. *Briefings in bioinformatics*, 17(5):877–890, 2016.
- [7] Hyunsoo Kim and Haesun Park. Sparse non-negative matrix factorizations via alternating non-negativity-constrained least squares for microarray data analysis. *Bioinformatics*, 23(12):1495–1502, 2007.
- [8] Daniel D Lee and H Sebastian Seung. Learning the parts of objects by non-negative matrix factorization. *Nature*, 401(6755):788, 1999.
- [9] Daniel D Lee and H Sebastian Seung. Algorithms for non-negative matrix factorization. In *Advances in neural information processing systems*, pp. 556–562, 2001.
- [10] John P McCutcheon and Carol D Von Dohlen. An interdependent metabolic patchwork in the nested symbiosis of mealybugs. *Current Biology*, 21(16):1366–1372, 2011.
- [11] Morgan N Price, Grant M Zane, Jennifer V Kuehl, Ryan A Melnyk, Judy D Wall, Adam M Deutschbauer, and Adam P Arkin. Filling gaps in bacterial amino acid biosynthesis pathways with high-throughput genetics. *PLoS genetics*, 14(1), 2018.
- [12] Alexander Sczyrba, Peter Hofmann, Peter Belmann, David Koslicki, Stefan Janssen, Johannes Dröge, Ivan Gregor, Stephan Majda, Jessika Fiedler, Eik Dahms, et al. Critical assessment of metagenome interpretation—a benchmark of metagenomics software. *Nature methods*, 14(11):1063, 2017.
- [13] Frank J Stewart, Adrian K Sharma, Jessica A Bryant, John M Eppley, and Edward F DeLong. Community transcriptomics reveals universal patterns of protein sequence conservation in natural microbial communities. *Genome biology*, 12(3):R26, 2011.

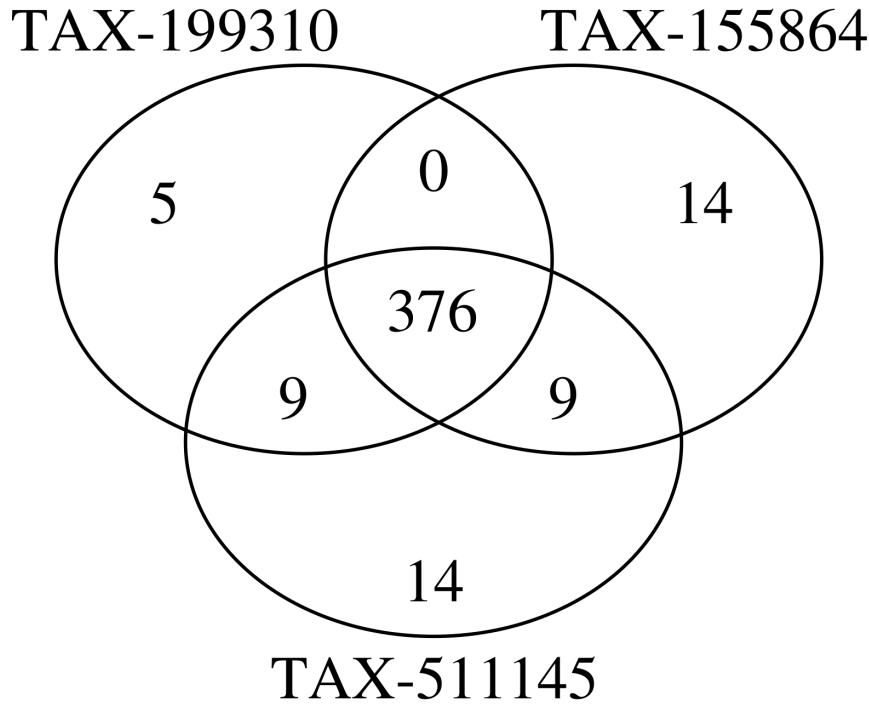


Figure 6: A three way set analysis of predicted pathways for E. coli K-12 substr. MG1655 (TAX-511145), E. coli str. CFT073 (TAX-199310), and E. coli O157:H7 str. EDL933 (TAX-155864) predicted by (a) PathoLogic (without taxonomic pruning) and (b) triUMPF.

Methods	Hamming Loss ↓					
	EcoCyc	HumanCyc	AraCyc	YeastCyc	LeishCyc	TrypanoCyc
PathoLogic	0.0610	<b>0.0633</b>	0.1188	<b>0.0424</b>	<b>0.0368</b>	<b>0.0424</b>
MinPath	0.2257	0.2530	0.3266	0.2482	0.1615	0.2561
mLGPR	0.0804	<b>0.0633</b>	<b>0.1069</b>	0.0550	0.0380	0.0590
triUMPF	<b>0.0435</b>	0.0954	0.1560	0.0649	0.0443	0.0776
Methods	Average Precision Score ↑					
	EcoCyc	HumanCyc	AraCyc	YeastCyc	LeishCyc	TrypanoCyc
PathoLogic	0.7230	<b>0.6695</b>	0.7011	0.7194	<b>0.4803</b>	<b>0.5480</b>
MinPath	0.3490	0.3004	0.3806	0.2675	0.1758	0.2129
mLGPR	0.6187	0.6686	0.7372	0.6480	0.4731	0.5455
triUMPF	<b>0.8662</b>	0.6080	<b>0.7377</b>	<b>0.7273</b>	0.4161	0.4561
Methods	Average Recall Score ↑					
	EcoCyc	HumanCyc	AraCyc	YeastCyc	LeishCyc	TrypanoCyc
PathoLogic	0.8078	0.8423	0.7176	0.8734	0.8391	0.7829
MinPath	<b>0.9902</b>	<b>0.9713</b>	<b>0.9843</b>	<b>1.0000</b>	<b>1.0000</b>	<b>1.0000</b>
mLGPR	0.8827	0.8459	0.7314	0.8603	0.9080	0.8914
triUMPF	0.7590	0.3835	0.3529	0.3319	0.7126	0.6229
Methods	Average F1 Score ↑					
	EcoCyc	HumanCyc	AraCyc	YeastCyc	LeishCyc	TrypanoCyc
PathoLogic	0.7631	0.7460	0.7093	<b>0.7890</b>	0.6109	0.6447
MinPath	0.5161	0.4589	0.5489	0.4221	0.2990	0.3511
mLGPR	0.7275	<b>0.7468</b>	<b>0.7343</b>	0.7392	<b>0.6220</b>	<b>0.6768</b>
triUMPF	<b>0.8090</b>	0.4703	0.4775	0.4735	0.5254	0.5266

Table 4: **Predictive performance of each comparing algorithm on 6 benchmark datasets.** For each performance metric, ‘↓’ indicates the smaller score is better while ‘↑’ indicates the higher score is better.

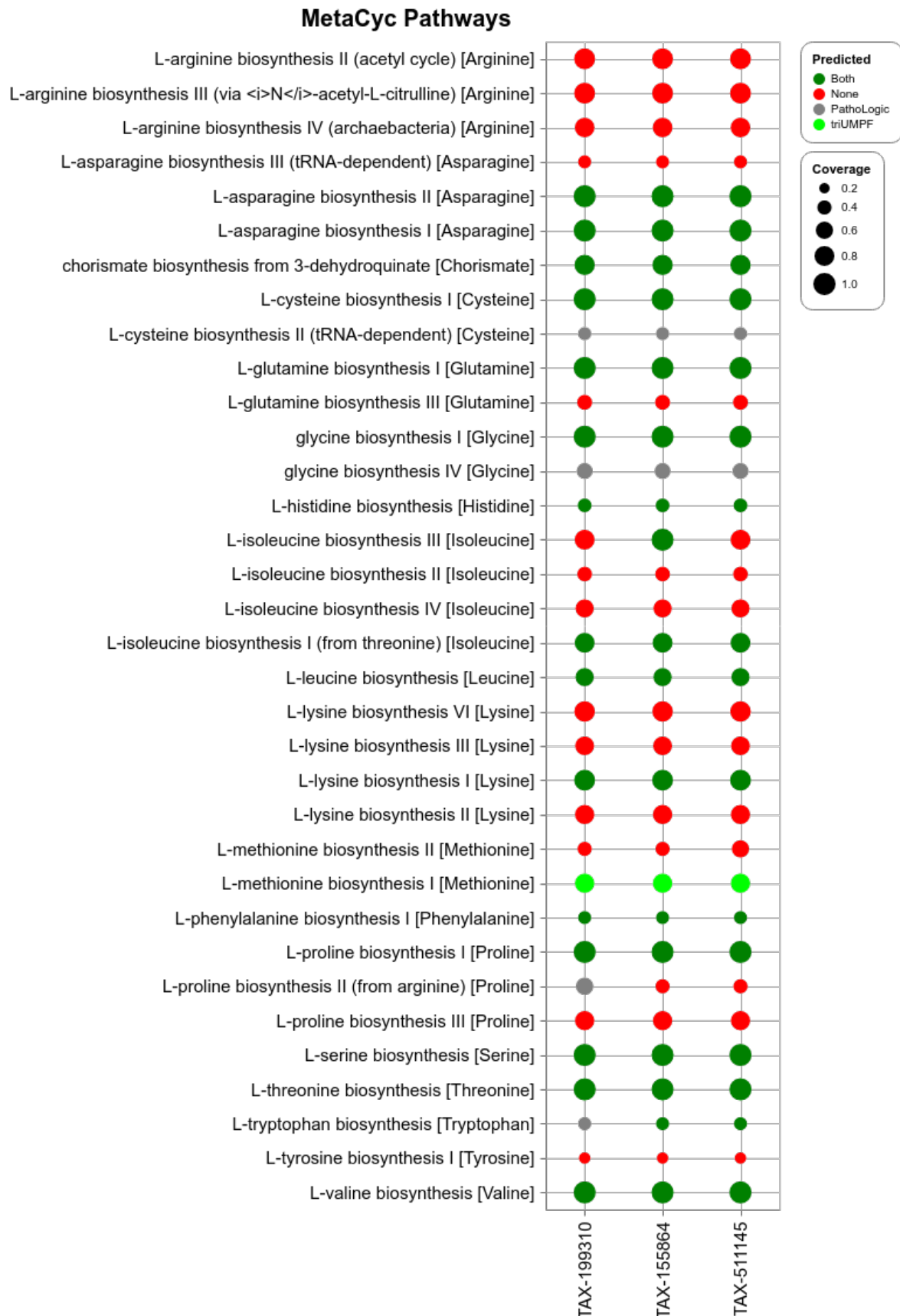


Figure 7: Comparison of predicted pathways for *E. coli* K-12 substr. MG1655 (TAX-511145), *E. coli* str. CFT073 (TAX-199310), and *E. coli* O157:H7 str. EDL933 (TAX-155864) datasets between PathoLogic (without taxonomic pruning) and triUMPF. Red circles indicate that neither method predicted a specific pathway while green circles indicate that both methods predicted a specific pathway. Lime circles indicate pathways predicted solely by mLGPR and gray circles indicate pathways solely predicted by PathoLogic. The size of circles corresponds to the associated coverage information.

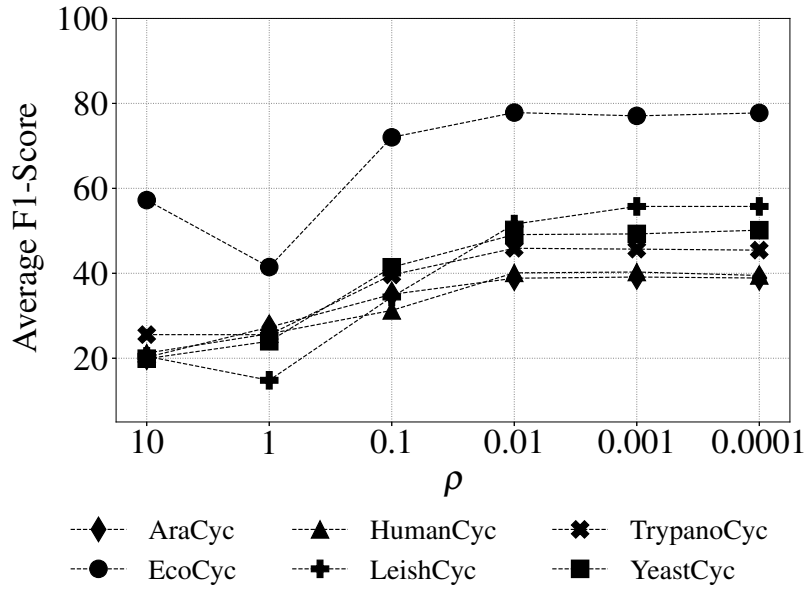


Figure 8: Effect of  $\rho$  based on average F1 score using golden datasets.

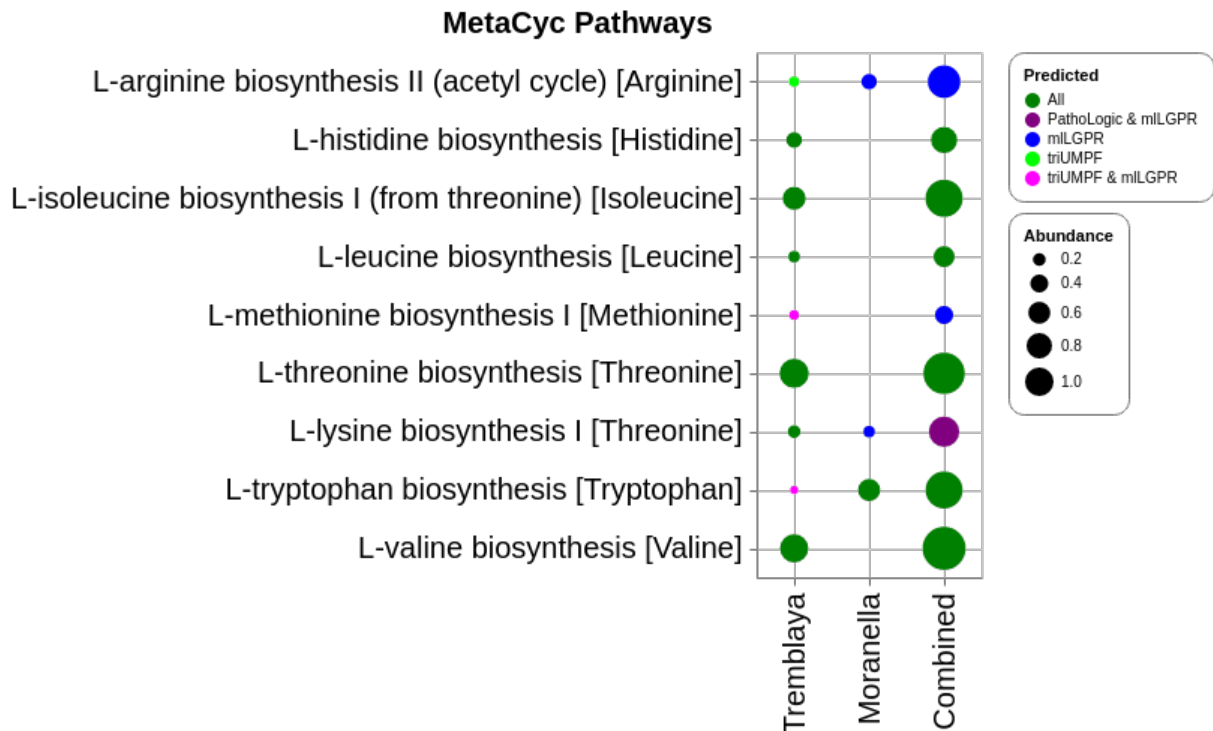


Figure 9: Comparative study of predicted pathways for symbiotic data between PathoLogic, mLGPR, and triUMPF. The size of circles corresponds the associated abundance information.

Metric	mLGPR	triUMPF
Hamming Loss ( $\downarrow$ )	0.0975	<b>0.0436</b>
Average Precision Score ( $\uparrow$ )	0.3570	<b>0.7027</b>
Average Recall Score ( $\uparrow$ )	<b>0.7827</b>	0.5101
Average F1 Score ( $\uparrow$ )	0.4866	<b>0.5864</b>

Table 5: Predictive performance of mLGPR and triUMPF on CAMI low complexity data.

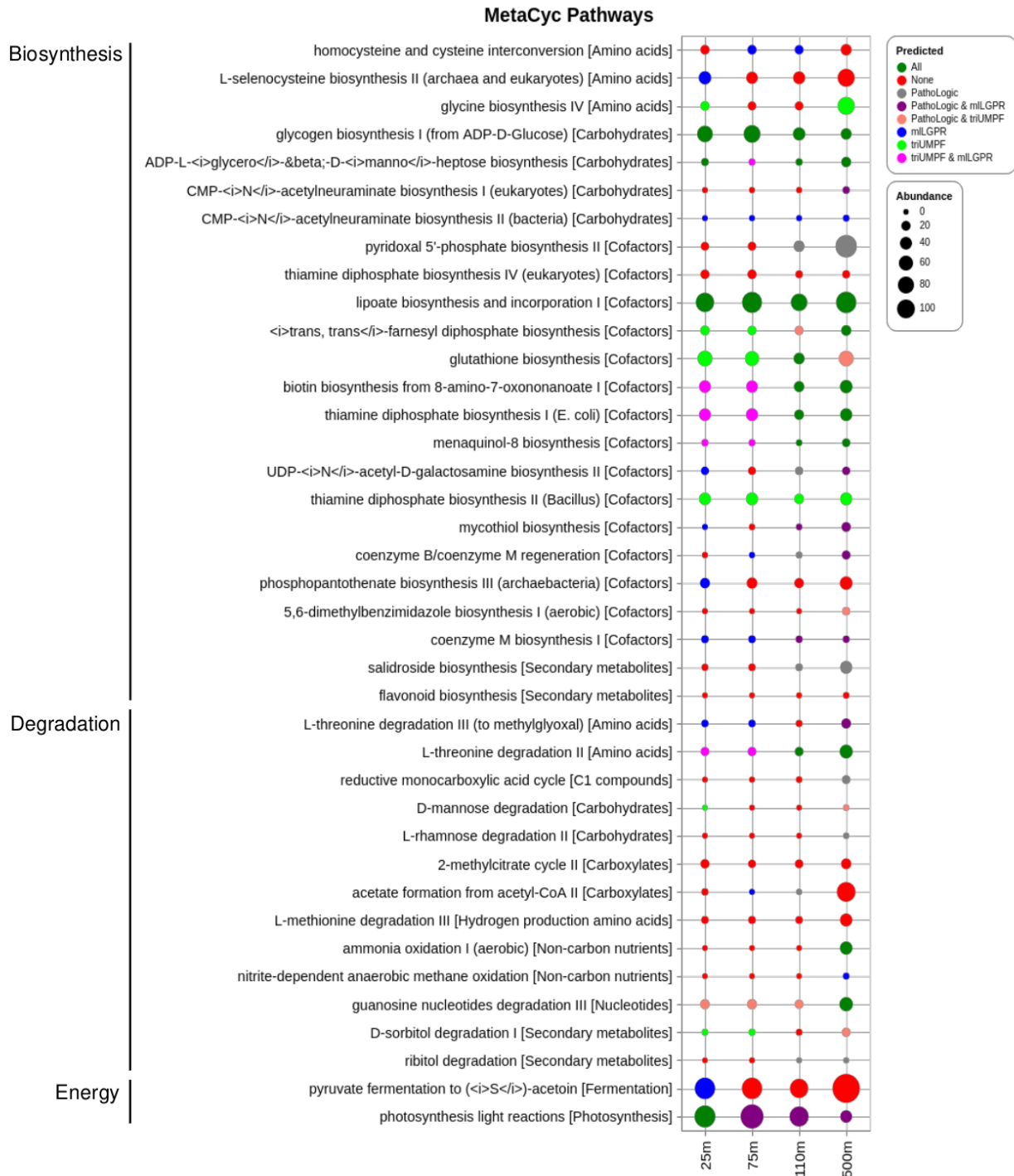


Figure 10: Comparative study of predicted pathways for HOT DNA samples. The size of circles corresponds the associated abundance information.